Deep-Learning-Based Approach for Estimation of Fractional Abundance of Nitrogen in Soil From Hyperspectral Data

Ajay Kumar Patel, *Student Member, IEEE*, Jayanta Kumar Ghosh, Shivam Pande, *Student Member, IEEE*, and Sameer Usmangani Sayyad

***Abstract*—One of the vital growth nutrient parameters of crops is soil Nitrogen (N) content. The ability to accurately grasp soil nutrient information is a prerequisite for scientific fertilization within the field of precision agriculture. Information pertaining to soil macronutrients, such as N, may be obtained quickly through hyperspectral imaging techniques. Objective of this research is to explore the use of a deep learning (DL) network to estimate the abundance of urea fertilizer mixed soils for spectroradiometer data. The proposed approach was tested for silt clay and loamy types of soils. Spectral regions of 1899.2 nm for urea and 2195.1 nm for soils were identified as optimum spectral absorption features. The accuracy evaluation was performed using a linear regression model between actual and estimated abundances. At 1899.2 nm, the coefficient of determination (R^2) for mixed samples of urea and silt clay soil was found to be 0.945, while R^2 for urea mixed loamy soil were 0.954. Similarly, at 2195.1 nm, R^2 obtained 0.953 for urea mixed silt clay soil and 0.944 for urea mixed loamy soil. The results show that the estimated abundances obtained through the derivative analysis for spectral unmixing (DASU)-based DL network facilitated a greater accuracy in comparison to the sole use of DASU. These results were then verified through conventional chemical analysis methods. The outcome of this article determines the abundance of urea mixed soils. Therefore, it is inferred that the hyperspectral imaging technique may be utilized *in-situ* to assess the agricultural land's soil fertility status.**

***Index Terms*—Deep learning (DL) network, hyperspectral remote sensing, precision agriculture, soil macronutrients, spectral unmixing.**

I. Introduction

AS DEFINITIVE measures of soil fertility, soil macronutrients play an essential role in sustainable development in agrarian productivity, food security, agricultural ecosystems, and precision agriculture [1]. Fertilization consistent with the richness or poorness of macronutrients in the soil is the basis for high-yield and high-quality agricultural products [2]. However, fertilization is often done mechanically or blindly to reap a high crop yield. The use of excessive fertilizer not only reduces the rate of fertilizer utilization and causes extreme macronutrient content in crops but also causes financial losses and severe environmental pollution [3]. Nitrogen (N) fertilizer is taken into consideration via growers as a primary macronutrient for plant growth and development because it is directly related to the photosynthesis process [4]. Subsequently, the optimization of N for different crops has emerged as a topic of many spectroscopic studies [5], [6]. Estimating N's soil composition is an effective way to optimize N fertilizer management and improve crop yield [7]. Computation of N composition in soil may be divided into two main types: destructive and nondestructive methods. Destructive methods for estimating soil macronutrients are laboratory-based chemical analysis tests [8]. However, these traditional methods are laborious, complicated, lengthy, and costly to operate. Also, acid-base waste may cause environmental pollution [9]–[11]. Researchers worldwide are attempting to develop ways for on-the-go *in-situ* sensing and assessment of soil properties, so as to optimize the amount of fertilizers applied. This will increase crop productivity while mitigating any detrimental environmental effects.

Consequently, researchers have sought real-time nondestructive methods for estimating the composition of N in soils. Hyperspectral technique is a nondestructive optical remote sensing technique, and it provides an abundance of spectral information, which recommends a potential approach for computing soil macronutrients. Hyperspectral data (due to their numerous contiguous bands) are particularly suited for *in-situ* measurements and can lower the required number of field samples and eliminate the need for chemical reagents [12]. Consequently, this will reduce the time and cost implications associated with field data collection and analysis. Thus, soil macronutrients can be analyzed in real-time over a larger spatial area [13], [14]. Therefore, hyperspectral remote sensing has attracted the attention of a wide range of recent agricultural studies [15]–[20], thus advocating for its continued use within precision agriculture. Several researchers have attested to the nondestructive capabilities of hyperspectral remote sensing in determining N fertilization levels within the soil [21]–[34]. Extensive reviews

Manuscript received May 1, 2020; revised August 3, 2020 and November 11, 2020; accepted November 17, 2020. Date of publication November 23, 2020; date of current version December 9, 2020. This work was supported in part by the Ministry of Human Resource Development, Government of India, India. *(Corresponding author: Ajay Kumar Patel.)*

Ajay Kumar Patel and Jayanta Kumar Ghosh are with the Geomatics Engineering Group, Indian Institute of Technology Roorkee, Roorkee 247667, India (e-mail: apatel1@ce.iitr.ac.in; gjkumfce@iitr.ac.in).

Shivam Pande is with the Centre of Studies in Resources Engineering, Indian Institute of Technology Bombay, Mumbai 400076, India (e-mail: shivam_pande@iitb.ac.in).

Sameer Usmangani Sayyad is with the Environmental Engineering Group, Indian Institute of Technology Roorkee, Roorkee 247667, India (e-mail: susayyad@ci.vjti.ac.in).

Digital Object Identifier 10.1109/JSTARS.2020.3039844

on the use of hyperspectral remote sensing for predicting soil properties can be found in [35]–[40].

Spectral unmixing is an essential step for categorizing the land cover classes of mixed pixels within hyperspectral data [41], [42]. In this process, the measured spectral reflectance curve (SRC) of a mixed study sample is decomposed into products of different pure spectra (endmembers) and their corresponding proportions (abundance coefficients), that implies the fraction of each endmember within the mixed pixel [43]. Endmembers may be collected from the study samples or obtained from readily available spectral data libraries [44]. Several studies have demonstrated the progression of spectral unmixing within the domain of hyperspectral remote sensing [45]–[51]. More precisely, the following approaches have been used widely for spectral unmixing, namely, mixing models, geometrical-based, sparse-regression-based, statistical-based, soft-classification-based, machine-learning-based, and the combination of spectral and spatial information [46], [52]. The contemporary spectral unmixing methods for soil macronutrients categorized into linear and or nonlinear mixing model (LMM/NLMM) [53]–[59]. The LMM constructs linear mathematical relationships between spectral variables derived from hyperspectral datasets and soil macronutrient contents [34], [31]. In LMM, the partial least squares regression and the multiple linear regressions are often used [60]–[62]. The NLMM assumes that the incident light follows multiple scattering phenomena [63]. Many researchers have used LMM and NLMM to analyze the spectral unmixing of hyperspectral data [64]–[70]. This article focuses on the spectral unmixing method with LMM. Because the LMM has simplicity and clear physical meaning, it is widely used for spectral unmixing of hyperspectral data [41].

Machine learning techniques that are efficient for handling large amounts of input variables have been tested for estimating the soil spectra [71]–[74]. These techniques, including artificial neural networks, random forests, back-propagation neural networks, and support vector machines, have been widely used to compute the compositions of soil and N fertilizer [75], [76]. Moreover, wavelength selection models have also been found competent [77], [78]. Neural networks are recognized as very effective techniques for spectral unmixing of hyperspectral data [79]–[81]. Further advancements in computing technology have encouraged the development of powerful deep learning (DL) techniques [82]. These techniques have demonstrated promising results in spectral unmixing of hyperspectral data [83]–[88].

The objective of this article is, therefore, to explore the use of a DL technique and *in situ* hyperspectral data in estimating the abundance of soil and urea fertilizer combinations. First, we introduced an integrated model of spectral derivative and spectral unmixing named derivative analysis for spectral unmixing (DASU) approach for estimating the abundances of mixed pixels of hyperspectral data. Second, we proposed a DASU-based DL network that was trained using the DASU estimated abundance. Third, we computed the abundance of compositions of soil and urea fertilizer in complex mixtures using the DASU alone and proposed the DASU-based DL network. Fourth, the accuracy assessment of the output of both approaches was examined. Eventually, the findings of the chemical analysis of mixed samples of urea fertilizer and soil were assessed.

II. Materials

A. Soil Sampling Sites

The two types of soil samples (loamy and silt clay based on the soil texture) used in this article were collected from Roorkee, Uttarakhand, India. The site for loamy soil is located 29° 51' N, 77° 54' E and for silt clay soil 29° 56' N, 78° 9' E [34]. The study region is at ∼268 m above sea level. The climate is a semi-humid continental type with an average annual temperature of about 23.7°C and relative humidity at ∼61%. Since soil macronutrients are mostly concentrated on the surface of the earth, soil samples were collected within the soil horizon at a depth of 15–20 cm, as per conventional soil sampling techniques [89]. Approximately 5 kg of each soil type was collected in a polythene bag, packed, labeled, and brought in the lab for further analysis. The soil samples were dried in an oven at 105°C for 24 h, taken after by grinding. A 2 mm sieve (IS No. 10) was used for the sieving to remove the study samples' unwanted impurities [90].

B. Inorganic Component

The commercially available inorganic urea fertilizer has been used, which contains 46% of N. The chemical formula of urea fertilizer is $CO(NH)_2$. Urea is the most abundant source of N among the conventional dry fertilizers. Nitrogenous fertilizers are manufactured and synthesized artificially in chemical industries. The principal source of N in fertilizers is ammonium nitrate, anhydrous ammonia, and urea [91]. Crops absorb N as a mineral nutrient mainly from the soil, and it is distributed in the form of nitrate (NO_3^-) and ammonium (NH_4^+) [92]. As compared to other soil nutrients, N is a limiting plant nutrient, which is required in higher concentrations (mmol/kg dry mass) to stimulate optimum crop growth.

C. Mixed Sample Preparation

Each soil sample was mixed with urea fertilizer at a definite composition to obtain a hyperspectral data with varying abundance of two soil types (loamy and silt clay) and urea fertilizer. A pure sample of each soil type and urea fertilizer along with the 15 mixed samples for each soil type were prepared, as shown in Fig. 1(a)–(d). Mixed samples were made using the dry, sieved soil along with urea fertilizer. In order to ensure a homogenous nature of the prepared mixed samples, it was kept at room temperature for four days prior to further analysis. The proportion of N in the urea fertilizer and mixed study samples was determined using conversion factor with their molecular mass. According to [93], 1.5 cm thick soil is considered as optically infinite soil; therefore, the mixed samples were kept in a rectangular plastic case with a profundity of 3 cm, as shown in Fig. 1(d). Among all the 100 gms of prepared samples, three pure study samples (two soil types and urea fertilizer) were used for qualitative analysis. Thirty mixed study samples were used to quantify the abundance of N and soil.

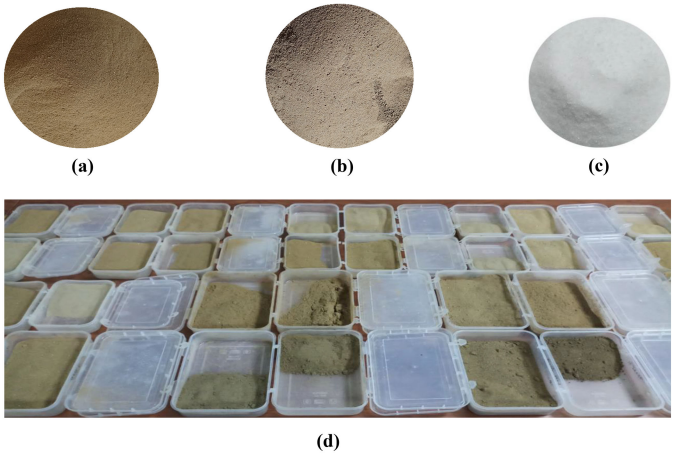

Fig. 1. Digital camera images of (a) loamy soil, (b) silt clay soil, (c) urea fertilizer, and (d) mixed study samples of soil, and urea fertilizer.

D. Spectral Data Acquisition

A portable spectroradiometer SVC XHR-1024i (manufactured by Spectra Vista Corporation) was used in the laboratory for the SRCs determination of the study samples. The spectroradiometer covers the visible to shortwave infrared (SWIR) wavelength range of 350 to 2500 nm with 994 bands. It is equipped with an improved spectral resolution of 2.8 nm at 700–1500 nm, 8 nm at 1500–2100 nm, and 6 nm at 2100–2500 nm. SRCs of three endmembers, two for each soil type and one for urea fertilizer are shown in Fig. 2(a). SRCs were acquired for prepared mixed samples ($n = 15$) of each soil type ($n = 2$) in 11 replicates, totaling to 330 scans. The average of 11 scans per study sample was calculated to minimize the instrumental noise and considered as final SRCs, as shown in Fig. 2(b) and (c). The SRCs of the study samples were imported through PC data acquisition software (SVC XHR-1024i) version 1.19.3. Two sets of abundances were generated from Dirichlet distribution, one for the combinations of urea fertilizer and pure silt clay soil and second for the combinations of pure loamy soil and urea fertilizer. A total number of 10 000 each mixed SCRs for both the datasets were generated to evaluate the performance of a DL network, as shown in Fig. 2(d) and (e). Additive zero-mean Gaussian noise with a signal-to-noise ratio set at 10, 20, and 30 dB is applied to the results.

III. Methodology

A. Spectral Derivative Features

Spectral derivatives of reflectance signatures may occupy prominent features of different constituents of the land surface. Such information has been utilized for the spectral unmixing of the hyperspectral remote sensing data along with SRCs [94]. Spectral derivative generally acquires the acute changes in the neighboring spectral bands, and such disparities may help to increase the efficiency of spectral unmixing by enhancing the absorption features in SRCs. The finite approximation was used to compute the spectral derivatives [95]. The benefit of finite approximation stems from its ability to estimate spectral resolutions at varying finite spectral resolutions, while extricating spectral features of interest [96]. A derivative of SRC is the rate of change of reflectance in relation to the spectral region of interest. The estimation of the first-order spectral derivative can be represented by the following equation:

$$\frac{\partial S}{\partial \lambda_k} = \frac{S(\lambda_k) - S(\lambda_l)}{\lambda_l - \lambda_k} \tag{1}$$

where S is the SRC and λ_k and λ_l are the wavelength regions of bands k and l. $S(\lambda_k)$ and $S(\lambda_l)$ are the reflectance values at wavelength regions of λ_k and λ_l. We assume $\lambda_l > \lambda_k$ without any loss of generality. The loss of spectral details and attenuation of significant spectral features in SRC may occur because of extensive spectral band separation $(\lambda_l - \lambda_k)$. Under other conditions, spectral band separation smaller than the instrument's spectral resolution may cause some aberration in the output. In this article, we adopt the second-order spectral derivative. High-order differentiation enhances excessive frequency noise while reducing small frequency background noise; subsequently, this effect may be amplified as the spectral derivative order increases.

B. Continuum Removal

To define the absorption characteristics of a material within a particular spectral region, assuming that no other component has high absorption characteristics around that wavelength, continuum removal (CR) is often applied [97]. The continuum is commonly estimated using local maxima to generate a hull of boundary points. All the boundary points are shaped by a straight line joining the two local spectral reflectance maxima of the peak absorption wavelength. Thus, CR was written as a function of spectral reflectance values at a particular region of wavelength, with the constraint that its maximum value could not exceed 1.0 [98].

C. Spectral Derivative Linear Mixing Model

Spectral unmixing seeks to evaluate the fractional abundance of the diverse materials occurring within the mixed pixels of hyperspectral data [99]. A classical approach for spectral unmixing is the linear mixing model, which assumes that the SRC of a mixed pixel is a linear combination of the constituent of the pure classes (endmembers) [100]. Linear mixing model is described by

$$S_m(\lambda) = \sum_{k=1}^{p} f_k es_k(\lambda) \tag{2}$$

$$\sum_{k=1}^{p} f_k = 1.0, \qquad 0 \le f_k \le 1.0 \tag{3}$$

where $S_m(\lambda)$ is the SRC of a mixed sample, $es_k(\lambda)$ is the SRC of kth endmember, f_k is the abundance of kth endmember in a mixed sample, and p are the endmembers that exist in the hyperspectral data [99]. If the endmembers present in mixed samples are linearly mixed, then its derivative will also follow the linearity [96]. Spectral derivative linear mixing model is

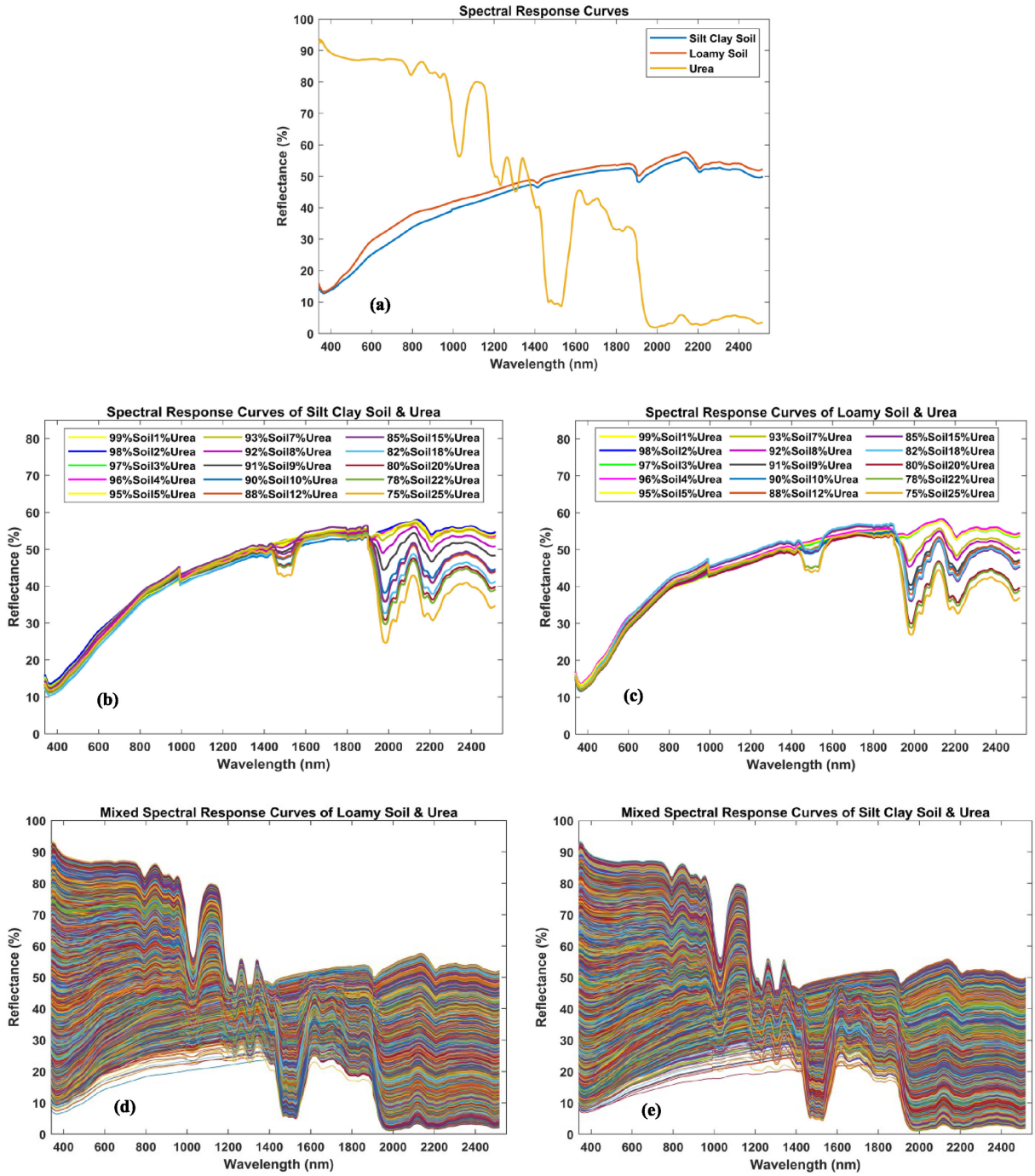

Fig. 2. SRCs of (a) two soil type and urea fertilizer, (b) mixed study samples of urea fertilizer and silt clay soil, (c) mixed study samples of urea fertilizer and loamy soil, (d) total number of 10 000 mixed pixels SRC of two endmembers (loamy soil and urea fertilizer), and (e) total number of 10 000 mixed pixels SRC of two endmembers (silt clay soil and urea fertilizer) are generated from Dirichlet distribution.

expressed by

$$\frac{\partial^n S_m(\lambda)}{\partial \lambda^n} = \sum_{k=1}^{p} \left(f_k \frac{\partial^n es_k(\lambda)}{\partial \lambda^n} \right) \tag{4}$$

where $\partial^n S_m(\lambda)/\partial\lambda^n$ is the nth-order-derivative SRC of a study mixed sample, $\partial^n es_k(\lambda)/\partial\lambda^n$ is the nth-order-derivative SRC of the kth endmember ($es_k(\lambda)$), f_k is the fractional abundance of the kth endmember in the study mixed sample. The advantage of the spectral derivative is the ability to resolve absorption features and determine their characteristic shapes and specific wavelength region. These absorption features are related to the SRCs of land cover classes; consequently, the endmembers and their abundance present in a mixed sample may be estimated. It may be needed to select more than one wavelength position to compute the fractional abundance of a mixed SRC which have more than two endmembers. Equation (4) can be used to determine the fractional abundance (f_k) of each selected endmember

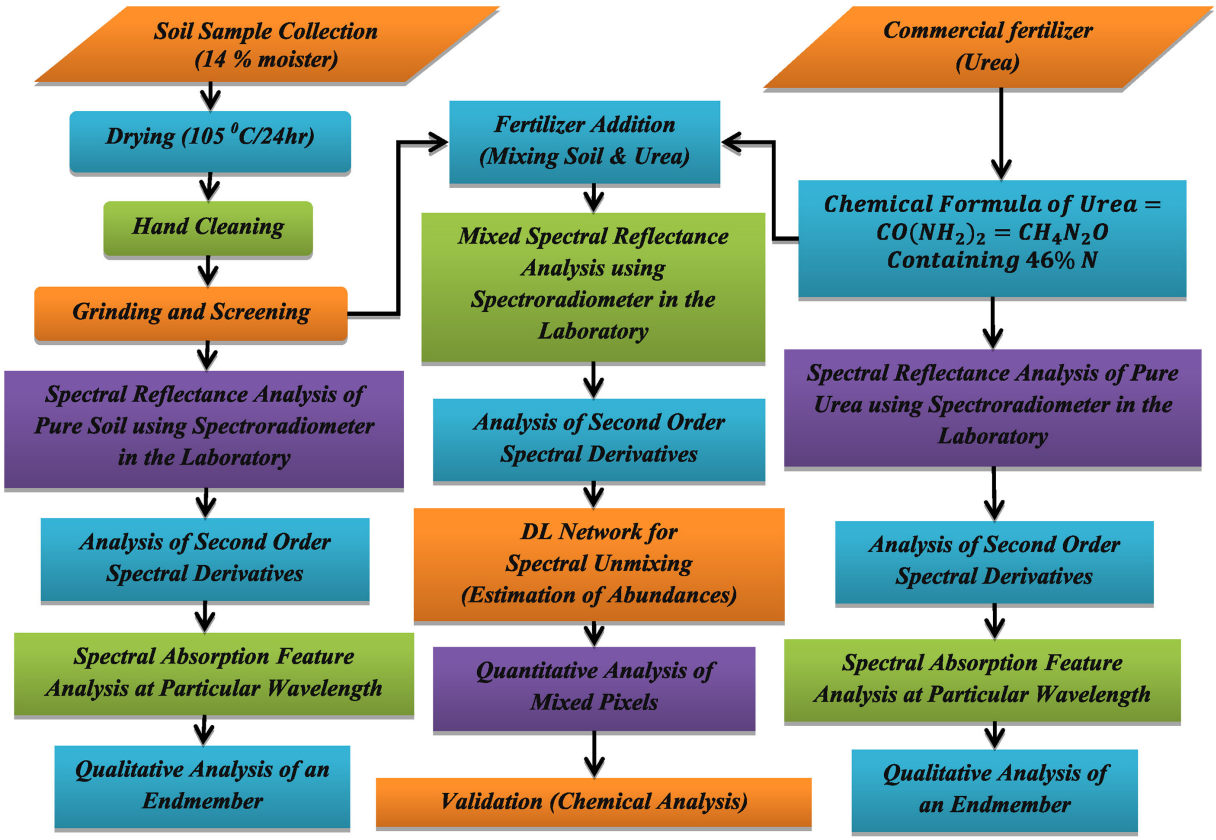

Fig. 3. Flow diagram of the DASU employed to estimation of abundance of composition of soil and urea fertilizer.

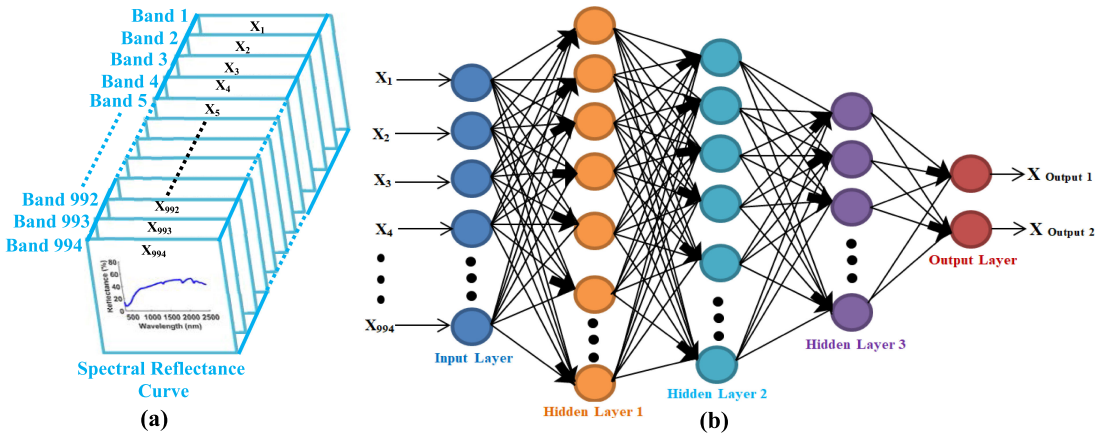

Fig. 4. (a) Input data: spectral reflectance curve. (b) Architecture of a fully connected DL network having one input layer with 994 nodes, three hidden layers with 2000, 1000, and 400 nodes, and an output layer with two nodes.

in an observed mixed pixel. In this article, a constrained linear unmixing approach (nonnegative and additivity) is employed as represented in (3) [101]. Fig. 3 expresses the flow diagram of the DASU technique, which was applied to compute the abundance of mixed soil and urea fertilizer samples.

D. Deep Learning Network

DL network was trained to estimate the abundance of mixed samples of urea fertilizer and soil. The DL network architecture is a multilayer perceptron such that the one input layer contains 994 nodes (spectral bands), three hidden layers with 2000, 1000, and 400 nodes, and an output layer with two nodes, as shown in Fig. 4(a) and (b). The dataset was divided into three categories, i.e., training, validation, and testing in order to train the network (70/15/15 split used). The training set was used to determine the parameters of the network (weights and biases). To train the algorithm, 10 000 mixed pixel SRCs of soil and urea fertilizer were generated using the Dirichlet distribution [70]. The validation set was used to minimize the over-fitting (generalization error). Thereafter, testing sets were used to test the final results of the network with the laboratory

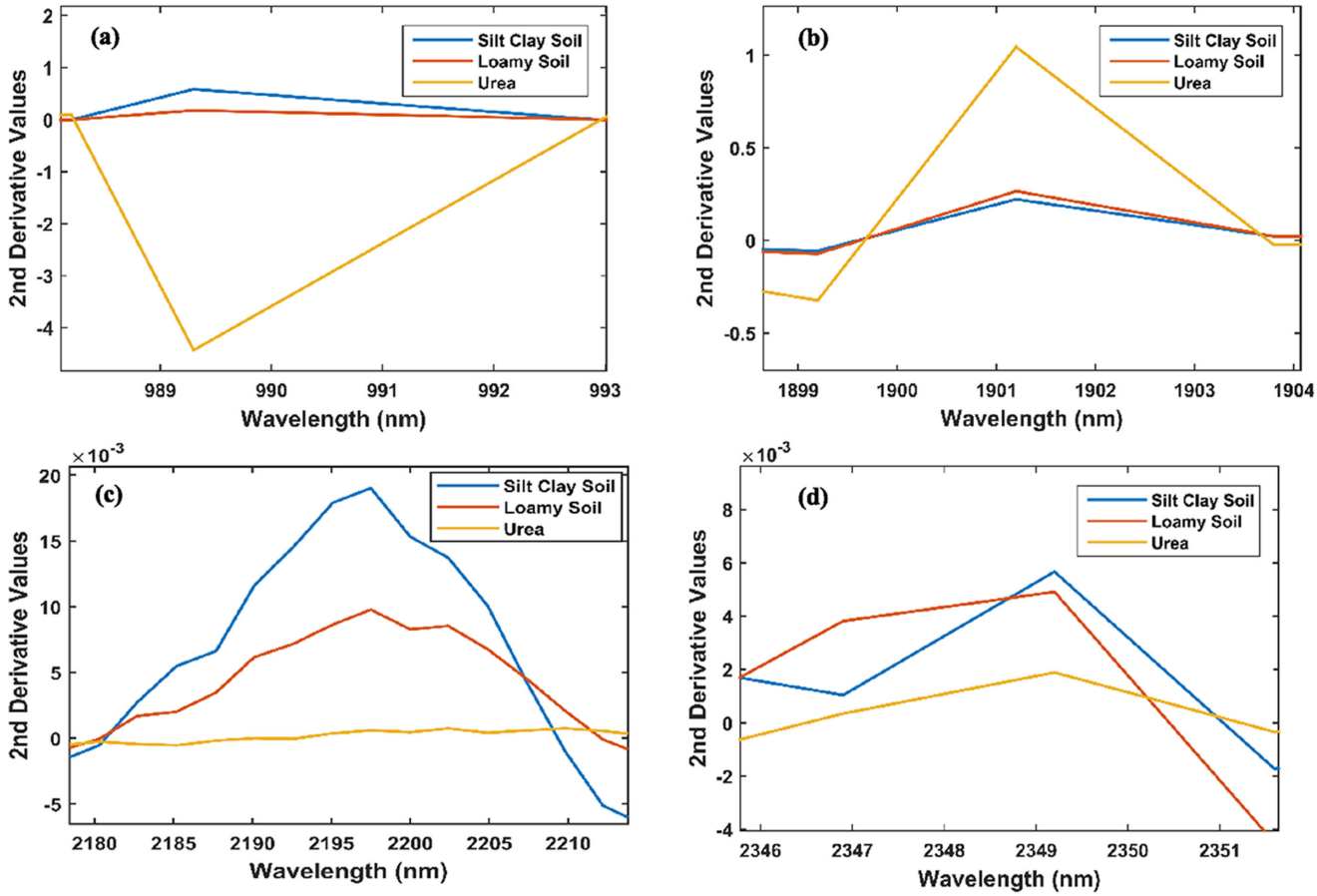

Fig. 5. Spectral derivative curves of urea fertilizer, silt clay soil, loamy soil at regions of wavelength (a) 989.3 nm, (b) 1899.2 nm, (c) 2195.1 nm, and (d) 2346.9 nm.

spectra results in order to evaluate the performance of the neural network [102].

E. Mixed Soil Sample Validation

In the laboratory, chemical analysis of study mixed samples was performed according to the standard method proposed by [103]. The 850 Professional Ion Chromatograph Anion-MCS (manufactured by Metrohm, Herisau, Switzerland) was used for computing the amount of inorganic N, as explained in [104]. Ion chromatography is a well-established technique, employed in the estimation of high or low molecular weight organic and inorganic ions, and ionizable organic compound [105]–[107]. Quantitative analysis of the output signal was processed using software named the MagIC Net 2.4 version (Metrohm).

IV. Results and Discussion

A. Optimum Wavelength for Estimation of Abundance

In general, changes in soil albedo and soil chromophores affect the characteristic spectral reflectance of the soil. Albedo is defined as the proportion of the incident light that is reflected by a surface, and it depends on the physical properties of the soil, such as texture, particle size, surface roughness, and moisture content. The chromophore is a chemical functional group that absorbs incident light. A change in soil chromophore is dependent on the chemical composition such as organic matter, iron oxides, and carbonates [108]–[111]. The most common iron-oxide minerals in the soil are goethite and hematite. These minerals are the main active components in the visible and near-infrared (VNIR) region (350–1000 nm) since various kinds of iron oxides cause the majority of electron transitions. Goethite and hematite minerals exhibit diagnostic spectral features in the VNIR region; therefore, the absorption bands are generally broad and smooth, as shown in Fig. 2(a) [112]. The three broad spectral absorption regions are mainly centered at around 1400, 1900, and 2200 nm [113]. These spectral absorption regions are due to O–H group in water molecules, aliphatic C–H group, and N–H group in amide [114]. Further, spectral absorption features include CO_3^{2-} in carbonate minerals at 2330 nm spectral region [115], Fe^{3+} and Fe^{2+} in iron oxide minerals between at around 500 to 900 nm wavelength regions [116], and various functional groups in organic matter throughout the entire spectral region 400 to 2500 nm [117]. A thorough delineation for each of the spectral absorption features are explained in [118]–[120]. Clay minerals in soil are chlorite, illite, kaolinite, and montmorillonite.

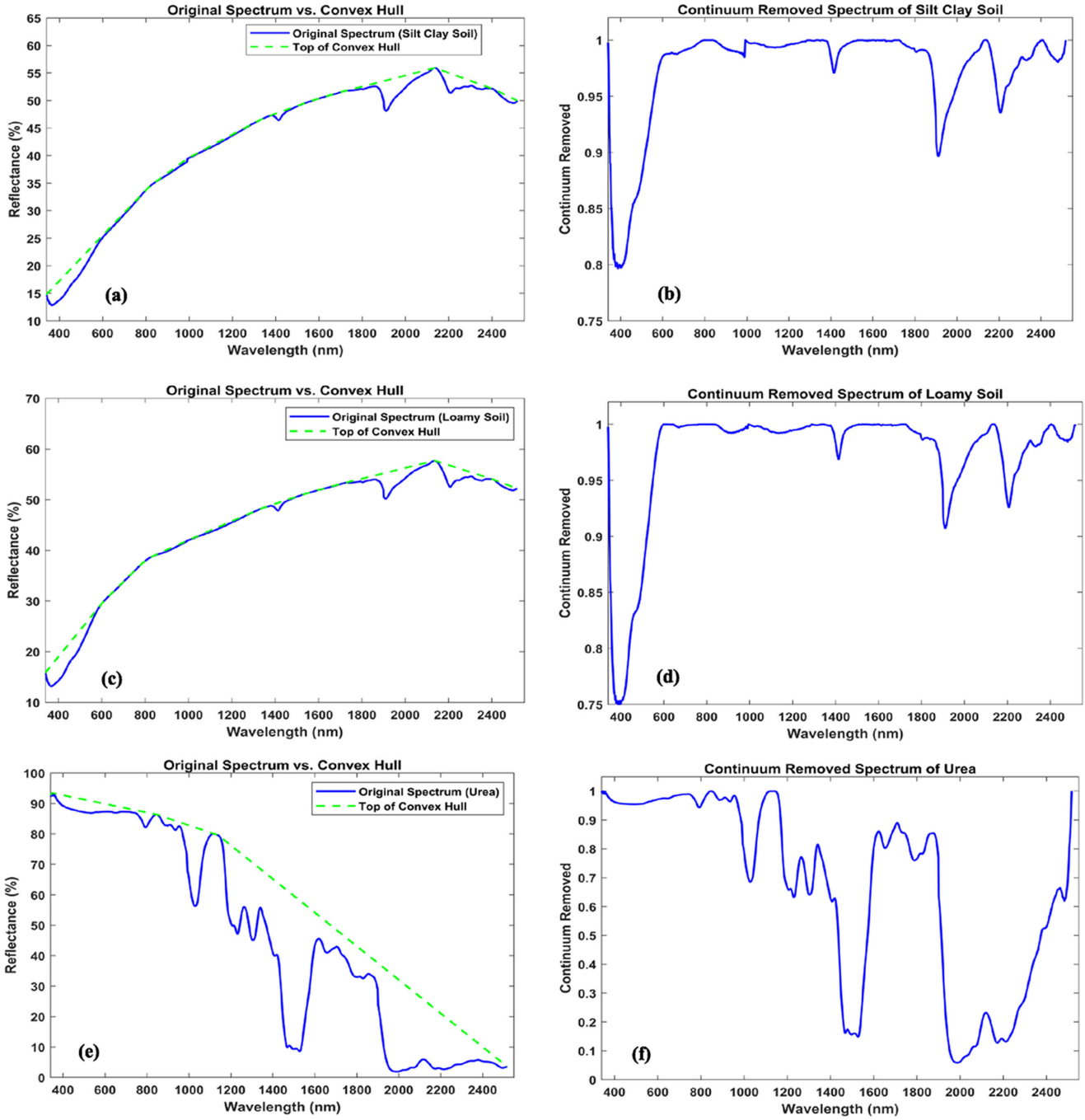

Fig. 6. (a) Continuum removal of the SRC of a silt clay type soil. (b) Continuum-removed SRC of a silt clay type soil. (c) Continuum removal of the SRC of a loamy type soil. (d) Continuum-removed SRC of a loamy type soil. (e) Continuum removal of the SRC of a urea fertilizer. (f) Continuum-removed SRC of a urea fertilizer.

The dominant clay type in soil shows diagnostic absorptions in the SWIR region (1500–2500 nm) [121]. These absorption bands are caused by the vibrational transitions, and commonly display sharp and narrow features, as shown in Fig. 2(a). Other few weak absorption bands in the 2300–2500 nm region are related to the presence of iron-hydroxide (Fe–OH) and/or magnesium hydroxide (Mg–OH) in the clay minerals [122]. The spectral derivative outcomes of SRCs for soil and urea fertilizer revealed significant absorption features, as shown in Fig. 5. Spectral derivative results for pure urea fertilizer show high positive peaks at 989.3 and 1899.2 nm wavelength regions since these wavelength regions are related to the amide functional group, N–H [123]. Whereas, the spectral derivative results of soils appear negative with short peaks at these wavelength regions, as shown in Fig. 5(a) and (b). Similarly, the spectral derivative results of all soil types display positive high peaks at 2195.1 and 2346.9 nm spectral regions due to the presence of clay minerals within the soil [124]. On the contrary, the spectral derivative

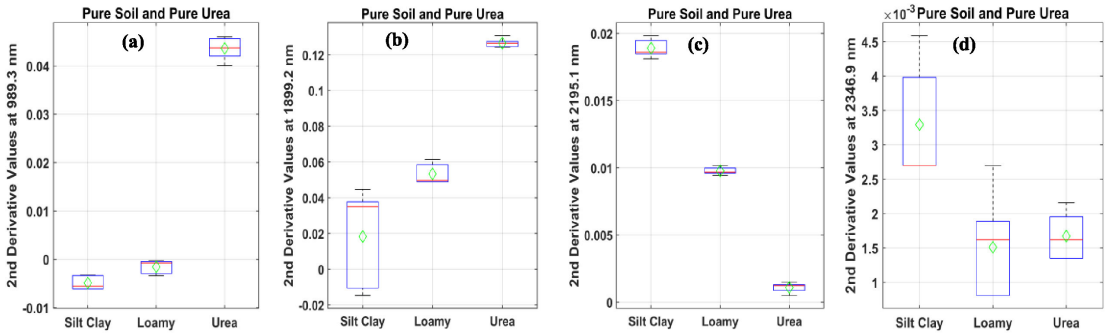

Fig. 7. Box plots of spectral derivative results of silt clay type soil, loamy type soil, and urea fertilizer at regions of wavelength (a) 989.3 nm, (b) 1899.2 nm, (c) 2195.1 nm, and (d) 2346.9 nm.

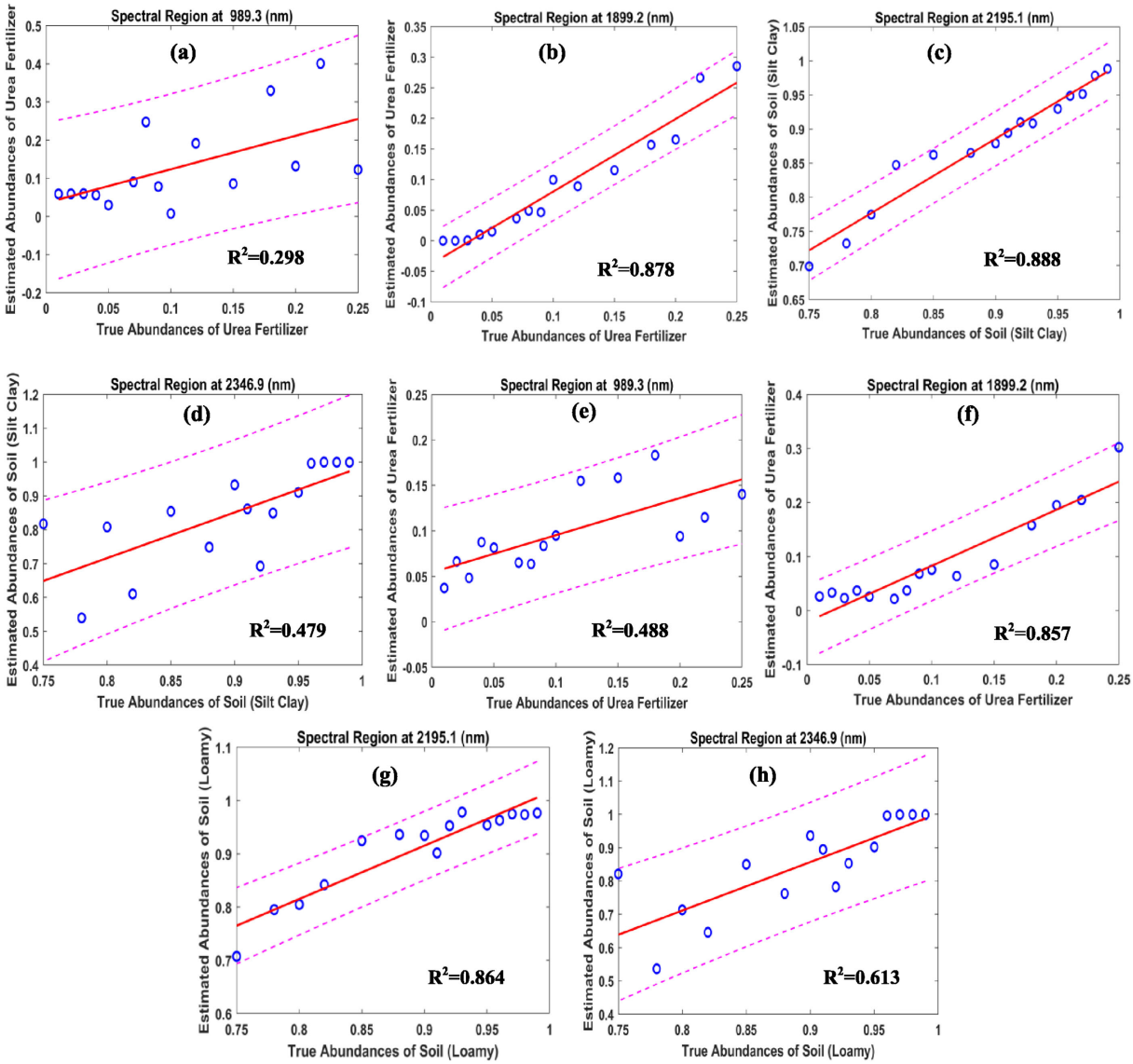

Fig. 8. Linear regression between the actual abundance and DASU alone estimated abundance at different wavelength regions. (a) At 989.3 nm, for abundance of urea fertilizer with silt clay type soil. (b) At 1899.2 nm, for abundance of urea fertilizer with silt clay type soil. (c) At 2195.1 nm, for abundance of silt clay type soil with urea fertilizer. (d) At 2346.9 nm, for abundance of silt clay type soil with urea fertilizer. (e) At 989.3 nm, for abundance of urea fertilizer with loamy type soil. (f) At 1899.2 nm, for abundance of urea fertilizer with loamy type soil. (g) At 2195.1 nm, for abundance of loamy type soil with urea fertilizer. (h) At 2346.9 nm, for abundance of loamy type soil with urea fertilizer.

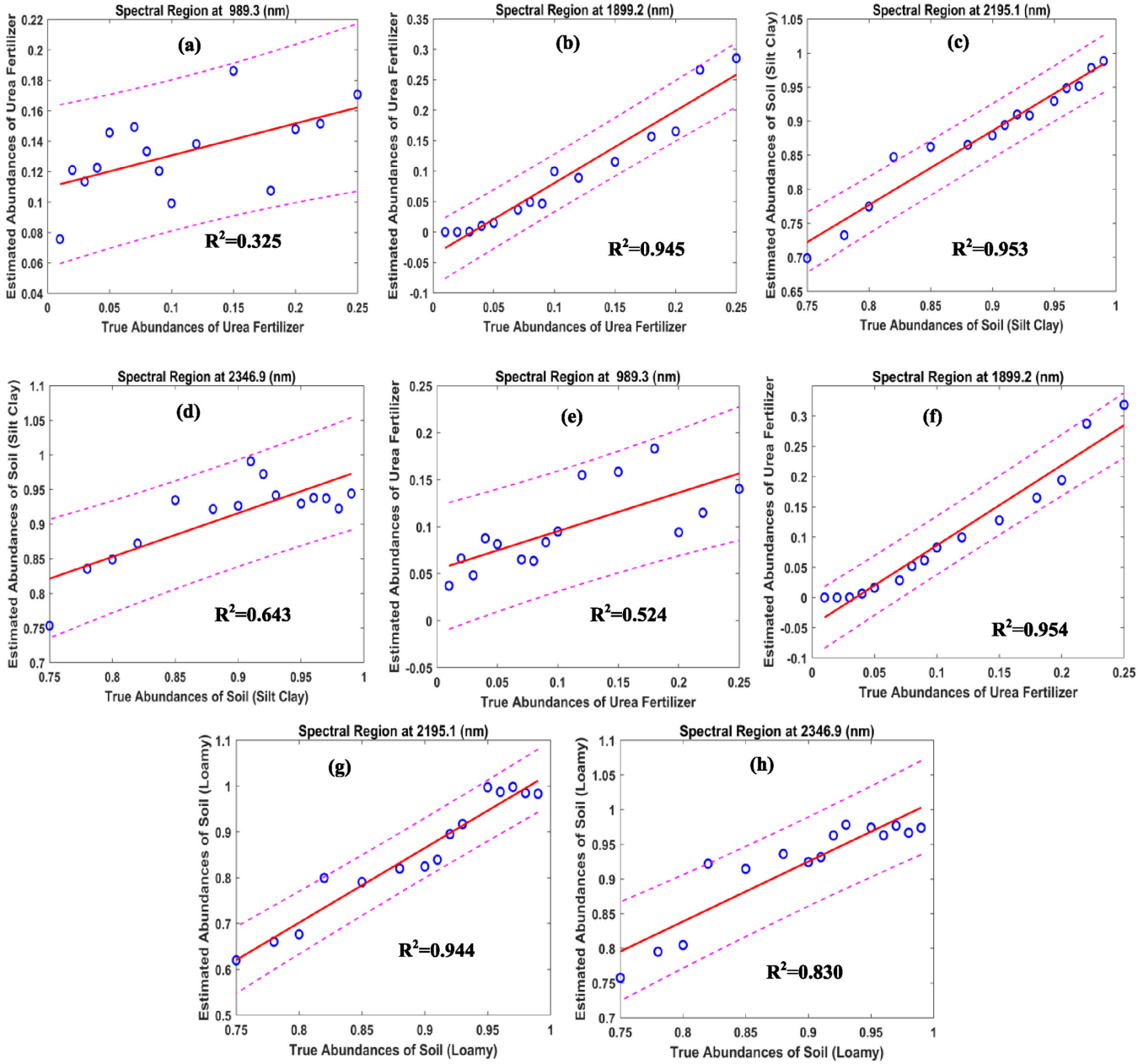

Fig. 9. Linear regression between the actual abundance and DASU-based DL network estimated abundance at different wavelength regions. (a) At 989.3 nm, for abundance of urea fertilizer with silt clay type soil. (b) At 1899.2 nm, for abundance of urea fertilizer with silt clay type soil. (c) At 2195.1 nm, for abundance of silt clay type soil with urea fertilizer. (d) At 2346.9 nm, for abundance of silt clay type soil with urea fertilizer. (e) At 989.3 nm, for abundance of urea fertilizer with loamy type soil. (f) At 1899.2 nm, for abundance of urea fertilizer with loamy type soil. (g) At 2195.1 nm, for abundance of loamy type soil with urea fertilizer. (h) At 2346.9 nm, for abundance of loamy type soil with urea fertilizer.

result of urea fertilizer shows an almost linear shape; thus, the derivative values are closer to zero at these wavelength regions, as shown in Fig. 5(c) and (d).

The CR spectra of both soil type and urea fertilizer are shown in Fig. 6. CR spectra may be used to identify and isolate the characteristic absorptions features of macronutrients, minerals, and water in soil [125]. The output of CR spectra for both the soil types revealed high absorption peaks near 1400, 1900, 2200, and 2350 nm, as shown in Fig. 6(a)–(d). Similarly, the CR spectra of urea fertilizer generate high absorption features near 1000, 1500, and 1950 nm, as shown in Fig. 6(e) and (f).

Box plots were calculated for the spectral derivative results based on an average of seven pure SRCs of each study endmembers (i.e., seven pure SRCs of loamy soil, seven pure SRCs of silt clay soil, and seven pure SRCs of urea), as shown in Fig. 7. The outcomes of mean, median, minima, maxima, and standard deviation of the spectral derivative values revealed that SRC of a urea fertilizer dominates at 989.3 and 1899.2 nm wavelength regions, as shown in Fig. 7(a) and (b). Whereas SRCs of both soils are overrepresented at 2195.1 and 2346.9 nm wavelength regions, as represented in Fig. 7(c) and (d). As per the above findings, spectral absorption features at 989.3 and 1899.2 nm

wavelength regions were selected for further estimation of the abundance of urea fertilizer present in the mixed study samples. Similarly, spectral absorption features at 2195.1 and 2346.9 nm wavelength regions were selected for further evaluation of the abundance of soils present in the mixed study samples. Unique spectral absorption features (dominating spectral region) has been selected to distinguish urea fertilizer from the two soil types.

The spectroradiometer data was analyzed using the DASU approach. The fractional abundances were estimated at 989.3, 1899.2, 2195.1, and 2346.9 nm wavelength regions for 30 mixed samples prepared in the laboratory, which are composite of each soil type and urea fertilizer using (4). For synthetically generated 10 000 mixed pixels, the abundance of soil and urea fertilizer was estimated at the aforementioned wavelength regions. The DASU estimated abundances were used to train the DL network. Finally, using a trained DL network, the fractional abundances of study mixed samples (laboratory samples) were estimated and compared with actual abundance. Further, the computed abundances of study mixed samples were used to evaluate the performance of the DASU and DASU-based DL network. The correlation between the DASU computed, and real abundance for 30 mixed samples were examined using the ordinary least square (parametric regression) model, as shown in Fig. 8. The coefficient of determination (R^2) for mixed samples containing silt clay soil type along with urea fertilizer was 0.298 at 989.3 nm, 0.878 at 1899.2 nm, 0.888 at 2195.1 nm, and 0.479 at 2346.9 nm, respectively. Similarly, R^2 results for the mixed samples containing loamy soil type with urea fertilizer were 0.488 at 989.3 nm, 0.864 at 1899.2 nm, 0.857 at 2195.1 nm, and 0.613 at 2346.9 nm. These results suggest that the DASU computed abundance for all endmembers yield the least variation at 1899.2 nm for urea fertilizer and 2195.1 nm for both soil types, as compared with the actual abundance $(0 < \text{slope} < 1)$, and formed a linear correlation among themselves, as depicted in Fig. 8(b), (c), (f), and (g). On the other hand, the DASU computed abundance yield relatively higher differences at 989.3 nm for urea fertilizer and 2346.9 nm for both soil type, as compared to the actual abundance $(\text{slope} > 2)$, and formed a nonlinear correlation between them, as shown in Fig. 8(a), (d), (e), and (h).

The DL network used in this article has one input layer (994 nodes), three hidden layers (2000, 1000, 400 nodes), and an output layer (two nodes). The rectified linear unit was used as an activation function [126] and stochastic gradient descent with 0.005 learning rate as an optimizer. The training was done for 1000 epochs. The correlations between the network computed abundance and the actual abundance was analyzed using a parametric regression model, as shown in Fig. 9. The R^2 for mixed study samples containing urea fertilizer and silt clay soil type was 0.325 at 989.3 nm, 0.945 at 1899.2 nm, 0.953 at 2195.1, and 0.643 at 2346.9 nm. Similarly, R^2 for mixed study samples containing urea fertilizer and loamy soil type was 0.524 at 989.3 nm, 0.954 at 1899.2 nm, 0.944 at 2195.1, and 0.83 at 2346.9 nm. These results suggest that the DASU-based DL network computed abundance for all the endmembers yield negligible variation at 1899.2 nm for urea fertilizer and 2195.1 nm for both soil types, as compared with the actual

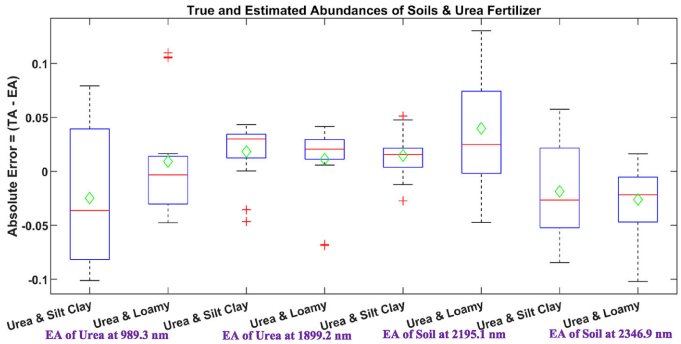

Fig. 10. Box plots for relative error distribution computed by subtracting the DASU-based DL network estimated abundance from the actual abundance of mixed study samples at 989.3, 1899.2, 2195.1, and 2346.9 nm wavelength regions.

abundance $(0 < \text{slope} < 1)$, and formed a linear correlation among themselves, as depicted in Fig. 9(b), (c), (f), and (g). In contrast, the DASU-based DL network computed abundance at 989.3 nm for urea fertilizer and 2346.9 nm for both soil type, yield relatively higher differences, as compared to the actual abundance $(\text{slope} > 2)$, and formed a nonlinear correlation between them, as shown in Fig. 9(a), (d), (e), and (h).

The salient features of the observed results are 1) the DASU and DASU-based DL network computed abundance for urea fertilizer gives better results at 1899.2 nm as compared to 989.3 nm, 2) the DASU and DASU-based DL network calculated abundance for the two soil types provide better results at 2195.1 nm as compared to 2346.9 nm. The results for DASU and DASU-based DL network estimated abundance at optimal wavelength for both the soil types are shown in Tables I– IV. A relatively significant R^2 values for DASU-based DL network computed abundance as compared to DASU alone suggests that the later approach is more efficient as compared to the former. The relative errors for DASU-based DL network computed abundance was calculated by subtracting the estimated abundance from the actual abundance of mixed study samples (Fig. 10, Tables III and IV).

In this article, a constrained linear unmixing approach (nonnegative and additivity) was used for the spectral unmixing process. All estimated abundance of mixed study samples were assumed only positive to follow the nonnegative constrained ($f_k \geq 0,\ k = 1, \ldots, p$), and the summation of the abundance of mixed study samples were taken equal to one to follow the additivity constraint ($\sum f_k = 1,\ k = 1, \ldots, p$) [99]. Therefore, the DASU-based DL network computed abundance has pursued the constraints at 1899.2 and 2195.1 nm wavelength regions for analysis of mixed study samples of urea fertilizer and both soil type, respectively. Consequently, (5) and (6) may provide an estimation of abundance in mixed samples of urea fertilizer and both soil types:

$$f_{\text{Urea\_estimate}} \approx \frac{\partial^2 S_m/\partial\lambda^2}{\partial^2 S_{\text{NPK}}/\partial\lambda^2} \quad \text{at } 1899.2 \text{ nm} \tag{5}$$

$$f_{\text{soil\_estimate}} \approx \frac{\partial^2 S_m/\partial\lambda^2}{\partial^2 S_{\text{soil}}/\partial\lambda^2} \quad \text{at } 2195.1 \text{ nm}. \tag{6}$$

TABLE I
RELATIVE ERROR WAS ESTIMATED FOR THE MIXED STUDY SAMPLES OF UREA FERTILIZER AND SILT CLAY SOIL TYPE BY SUBTRACTING THE DASU ESTIMATED ABUNDANCE (EA) FROM THE ACTUAL ABUNDANCE (AA) AT DIFFERENT WAVELENGTH REGIONS

Mixtures (g/100g)	AA1 Soil (%)	AA2 Urea (%)	Wavelength = 1899.2 nm		Wavelength = 2195.1 nm	
			EA1 Urea (%)	Error (%) (AA2-EA1)	EA2 Soil (%)	Error (%) (AA1-EA2)
Sample 1	0.99	0.01	0.001	0.009	0.966	0.024
Sample 2	0.98	0.02	0.004	0.016	0.947	0.033
Sample 3	0.97	0.03	0.006	0.024	0.961	0.009
Sample 4	0.96	0.04	0.009	0.031	0.961	-0.001
Sample 5	0.95	0.05	0.026	0.024	0.966	-0.016
Sample 6	0.93	0.07	0.022	0.048	0.989	-0.059
Sample 7	0.92	0.08	0.037	0.043	0.962	-0.042
Sample 8	0.91	0.09	0.068	0.022	0.956	-0.046
Sample 9	0.90	0.10	0.076	0.024	0.810	0.090
Sample 10	0.88	0.12	0.064	0.056	0.795	0.085
Sample 11	0.85	0.15	0.085	0.065	0.759	0.091
Sample 12	0.82	0.18	0.238	-0.058	0.736	0.084
Sample 13	0.80	0.20	0.195	0.005	0.707	0.092
Sample 14	0.78	0.22	0.325	-0.105	0.659	0.121
Sample 15	0.75	0.25	0.367	-0.117	0.600	0.150

TABLE II
RELATIVE ERROR WAS ESTIMATED FOR THE MIXED STUDY SAMPLES OF UREA FERTILIZER AND LOAMY SOIL TYPE BY SUBTRACTING THE DASU ESTIMATED ABUNDANCE (EA) FROM THE ACTUAL ABUNDANCE (AA) AT DIFFERENT WAVELENGTH REGIONS

Mixtures (g/100g)	AA1 Soil (%)	AA2 Urea (%)	Wavelength = 1899.2 nm		Wavelength = 2195.1 nm	
			EA1 Urea (%)	Error (%) (AA2-EA1)	EA2 Soil (%)	Error (%) (AA1-EA2)
Sample 1	0.99	0.01	0.026	-0.016	0.977	0.013
Sample 2	0.98	0.02	0.033	-0.013	0.974	0.006
Sample 3	0.97	0.03	0.023	0.007	0.975	-0.005
Sample 4	0.96	0.04	0.037	0.003	0.963	-0.003
Sample 5	0.95	0.05	0.026	0.024	0.954	-0.004
Sample 6	0.93	0.07	0.022	0.048	0.978	-0.048
Sample 7	0.92	0.08	0.037	0.043	0.953	-0.033
Sample 8	0.91	0.09	0.068	0.022	0.902	0.008
Sample 9	0.90	0.10	0.076	0.024	0.934	-0.034
Sample 10	0.88	0.12	0.064	0.056	0.936	-0.056
Sample 11	0.85	0.15	0.085	0.065	0.925	-0.075
Sample 12	0.82	0.18	0.158	0.022	0.842	-0.022
Sample 13	0.80	0.20	0.195	0.005	0.805	-0.005
Sample 14	0.78	0.22	0.205	0.015	0.795	-0.015
Sample 15	0.75	0.25	0.302	-0.052	0.708	0.042

In the processing of the DASU model alone and the DASU-based DL network requires at least one input SRC of each land cover class. In this article, we have used two soil types and urea fertilizer. All of these SRCs were spread across the wavelength region of 350–2500 nm. However, based on the analysis of spectral features of these SRCs, wavelength regions of 1899.2 and 2195.1 nm were selected for a qualitative investigation of endmembers of urea fertilizer and soil, followed by a constrained linear unmixing approach. Last, it was found that the DASU-based DL network functions well for the computation of abundances of mixed study samples at 1899.2 and 2195.1 nm wavelength regions. Therefore, these experimental

TABLE III
RELATIVE ERROR WAS ESTIMATED FOR THE MIXED STUDYS OF UREA FERTILIZER AND SILT CLAY SOIL TYPE BY SUBTRACTING THE DASU-BASED DL NETWORK EVALUATED ABUNDANCE (EA) FROM THE ACTUAL ABUNDANCE (AA) AT DIFFERENT WAVELENGTH REGIONS

Mixtures (g/100g)	AA1 Soil (%)	AA2 Urea (%)	Wavelength = 1899.2 nm		Wavelength = 2195.1 nm	
			EA1 Urea (%)	Error (%) (AA2-EA1)	EA2 Soil (%)	Error (%) (AA1-EA2)
Sample 1	0.99	0.01	0.000	0.010	0.988	0.002
Sample 2	0.98	0.02	0.000	0.011	0.978	0.002
Sample 3	0.97	0.03	0.000	0.030	0.951	0.019
Sample 4	0.96	0.04	0.009	0.030	0.948	0.011
Sample 5	0.95	0.05	0.014	0.035	0.929	0.020
Sample 6	0.93	0.07	0.036	0.033	0.908	0.022
Sample 7	0.92	0.08	0.049	0.030	0.909	0.010
Sample 8	0.91	0.09	0.046	0.043	0.894	0.016
Sample 9	0.90	0.10	0.099	0.000	0.879	0.021
Sample 10	0.88	0.12	0.089	0.031	0.865	0.015
Sample 11	0.85	0.15	0.115	0.035	0.862	-0.012
Sample 12	0.82	0.18	0.156	0.023	0.847	-0.027
Sample 13	0.80	0.20	0.165	0.035	0.774	0.025
Sample 14	0.78	0.22	0.266	-0.046	0.732	0.048
Sample 15	0.75	0.25	0.285	-0.035	0.698	0.051

TABLE IV
RELATIVE ERROR WAS ESTIMATED FOR THE MIXED STUDY SAMPLES OF UREA FERTILIZER AND LOAMY SOILT BY SUBTRACTING THE DASU-BASED DL NETWORK EVALUATED ABUNDANCE (EA) FROM THE ACTUAL ABUNDANCE (AA) AT DIFFERENT WAVELENGTH REGIONS

Mixtures (g/100g)	AA1 Soil (%)	AA2 Urea (%)	Wavelength = 1899.2 nm		Wavelength = 2195.1 nm	
			EA1 Urea (%)	Error (%) (AA2-EA1)	EA2 Soil (%)	Error (%) (AA1-EA2)
Sample 1	0.99	0.01	0.000	0.010	0.983	0.007
Sample 2	0.98	0.02	0.000	0.020	0.985	-0.005
Sample 3	0.97	0.03	0.001	0.030	0.998	-0.028
Sample 4	0.96	0.04	0.006	0.034	0.988	-0.027
Sample 5	0.95	0.05	0.016	0.034	0.997	-0.047
Sample 6	0.93	0.07	0.028	0.042	0.917	0.012
Sample 7	0.92	0.08	0.052	0.028	0.895	0.025
Sample 8	0.91	0.09	0.062	0.028	0.839	0.071
Sample 9	0.90	0.10	0.083	0.017	0.825	0.075
Sample 10	0.88	0.12	0.099	0.021	0.820	0.060
Sample 11	0.85	0.15	0.128	0.022	0.790	0.060
Sample 12	0.82	0.18	0.165	0.015	0.799	0.021
Sample 13	0.80	0.20	0.194	0.006	0.676	0.124
Sample 14	0.78	0.22	0.288	-0.068	0.660	0.120
Sample 15	0.75	0.25	0.319	-0.069	0.620	0.130

results revealed that the DASU-based DL network approach can be used for qualitative and quantitative analysis of mixed pixels hyperspectral data.

B. Verification

Chemical analysis for silt clay soil, urea fertilizer, and four mixed study samples was carried out using the well-known Ion Chromatography technique in the laboratory. The chemical analysis's motivation is to compute the amount of N in urea fertilizer, soil, and mixed study samples. We have calculated 46.6% N for g/100g sample in the study of urea fertilizer. The measure of N available in study samples was examined individually; also, the proportion of N in a mixed sample was estimated using conversion factors. The comprehensive assessment between the DASU-based DL network evaluated abundance and chemical analysis outcomes of the study mixed samples shows negligible differences, as presented in Table V.

TABLE V
DASU-BASED DL NETWORK AND CHEMICAL ANALYSIS RESULTS OF THE ABUNDANCE OF N INTIMATED WITH THE MIXTURES OF UREA FERTILIZER AND SILT CLAY SOIL TYPE

Mixtures (g/100g)	Actual abundance (%)	Network estimated abundance (%)		Chemical analysis (g/100g) (%)
		Wavelength at 1899.2 (nm)	Wavelength at 2195.1 (nm)	Examined from the study mixed sample
Sample 1 (98% Soil & 02% Urea)	$Urea = 2$ N=0.932	$Urea = 0.007$ N=0.003	$Urea = 2.16$ N=1.01	$Urea = 1.24$ N=0.58
Sample 2 (92% Soil & 08% Urea)	$Urea = 8$ N=3.728	$Urea = 4.92$ N=2.29	$Urea = 9.01$ N=4.20	$Urea = 6.42$ N=2.99
Sample 3 (88% Soil & 12% Urea)	$Urea = 12$ N=5.592	$Urea = 8.91$ N=4.15	$Urea = 13.49$ N=6.29	$Urea = 9.25$ N=4.31
Sample 4 (82% Soil &18% Urea)	$Urea = 18$ N=8.388	$Urea = 15.68$ N=7.31	$Urea = 15.27$ N=7.12	$Urea = 15.56$ N=7.25

The findings of the chemical analysis have been found that the N computed from the mixed study samples is less as compared to the N observed through the conversion factor.

V. CONCLUSION

In this article, the DASU approach, accompanied by the DL network, has been employed to estimate the abundance in mixed samples of soils and urea fertilizer using hyperspectral data. The DL algorithm can facilitate a greater accuracy for spectral unmixing of hyperspectral data. DL algorithms attempt to extract the endmembers and estimate the abundances of a mixed pixels. This article combines spectral derivative and spectral unmixing processes to demonstrate an unmixing model called DASU. The significant advantages of this technique are that spectral derivatives are important for the identification of endmembers as well as abundances of mixed samples, followed by linear spectral mixing model. Spectral derivative and CR analysis of SRCs of mixed samples provide various spectral absorption features to distinguish soils and urea fertilizer efficiently. The abundances of mixed soil samples for 10 000 synthetically generated mixed pixels were estimated using DASU approach. Furthermore, these abundances were used to train the DL network, after which, it was used to determine the fractional abundances of compositions of urea fertilizer and soils. Moreover, we have computed the abundances of mixed pixels originating from 30 combinations of soil and urea fertilizer using DASU alone. Following which, we compared the abundance results of the mixed soil samples estimated by only the DASU approach and the DASU-based DL network. The results of estimated abundance using both methods show that the wavelength regions of 1899.2 and 2195.1 nm were found optimal for the SRCs of urea fertilizer and soils, respectively. The accuracy assessment was performed through a linear regression model among the actual and estimated fractional abundance. The R^2 analysis of results of estimated abundances using both methods shows that the estimated abundances through the DASU-based DL network give better accuracy as compared to DASU alone.

The extensive investigation to identify the optimal spectral wavelength for computing the abundance of the mixed study samples at four wavelength regions (989.3, 1899.2, 2195.1, and 2346.9 nm) proclaimed the following:

1) The SRC of urea fertilizer shows higher reflectance at 1899.2 nm, as compared to 989.3 nm. Similarly, for both soil types, 2195.1 nm show a higher reflectance curve as compared to 2346.9 nm.
2) The spectral derivatives for urea fertilizer generate significant spectral absorption features at 1899.2 nm as compared to 989.3 nm. The spectral derivative for both soil types produces notable spectral absorption features at 2195.1 nm as compared to 2346.9 nm (Fig. 7).
3) The R^2 values calculated between the actual and DASU alone and the actual and DASU-based DL network estimated abundance for mixed study samples (Figs. 8 and 9) shows that the abundance estimated through DASU-based DL network gives better accuracy as compared to DASU alone.
4) The linear regression statistics of the actual and estimated abundance of mixed study samples for both approaches show that the abundance of urea fertilizer at 1899.2 nm has a significant difference as compared to 989.3 nm wavelength region. Likewise, the abundance of both soil types at 2195.1 nm has a significant difference as compared to 2346.9 nm wavelength region.
5) The box plot statistics of relative errors calculated between the actual and DASU-based DL network estimated abundance, as shown in Fig. 10, revealed that abundances of urea fertilizer at 1899.2 nm have less absolute errors as compared to 989.3 nm wavelength region. Likewise, abundances of both soil type at 2195.1 nm have less absolute errors as compared to 2346.9 nm wavelength region.

The results of the chemical analysis further support the DASU-based DL network as a powerful tool to estimate abundances using hyperspectral remote sensing data. The conclusion of the present article is that we have successfully developed a DASU-based DL network to determine the endmembers and quantify the abundance in a mixed study sample for hyperspectral data. For future development of the proposed algorithm may be the focus on the incorporation of the DL-based approaches (such as convolutional neural networks) into the DASU model.

ACKNOWLEDGMENT

The authors would like to acknowledge Prof. Raja Chowdhury, Assistant Professor, Environmental Engineering Group, Indian Institute of Technology Roorkee, India, for his guidance in laboratory-based chemical analysis. They would also like to

acknowledge Prof. Biplab Banerjee, Assistant Professor, Centre of Studies in Resources Engineering, Indian Institute of Technology Bombay, India, for his guidance in deep learning techniques. They would like to thanks anonymous reviewers for their careful reading of the manuscript and their many insightful comments and suggestions for improving the study.

REFERENCES

[1] B. Nowak, T. Nesme, C. David, and S. Pellerin, "Nutrient recycling in organic farming is related to diversity in farm types at the local level," *Agricultural Ecosyst. Environ.*, vol. 204, pp. 17–26, Jun. 2015.

[2] J. Chen *et al.*, "Environmentally friendly fertilizers: A review of materials used and their effects on the environment," *Sci. Total Environ.*, vol. 613–614, pp. 829–839, Feb. 2018.

[3] Y. Lu *et al.*, "Impacts of soil and water pollution on food safety and health risks in China," *Environ. Int.*, vol. 77, pp. 5–15, Apr. 2015.

[4] M. Andrews, J. A. Raven, and P. J. Lea, "Do plants need nitrate? The mechanisms by which nitrogen form affects plants," *Ann. Appl. Biol.*, vol. 163, no. 2, pp. 174–199, Sep. 2013.

[5] M. Quemada, J. Gabriel, and P. Zarco-Tejada, "Airborne hyperspectral images and ground-level optical sensors as assessment tools for maize nitrogen fertilization," *Remote Sens.*, vol. 6, no. 4, pp. 2940–2962, Mar. 2014.

[6] L. Liang *et al.*, "Estimation of leaf nitrogen content in wheat using new hyperspectral indices and a random forest regression algorithm," *Remote Sens.*, vol. 10, no. 12, Dec. 2018, Art. no. 1940.

[7] S. Xiao, Y. He, T. Dong, and P. Nie, "Spectral analysis and sensitive waveband determination based on nitrogen detection of different soil types using near infrared sensors," *Sensors*, vol. 18, no. 2, Feb. 2018, Art. no. 523.

[8] A. Mehlich, "Mehlich 3 soil test extractant: A modification of Mehlich 2 extractant," *Commun. Soil Sci. Plant Anal.*, vol. 15, no. 12, pp. 1409–1416, Dec. 1984.

[9] D. I. H. Jones and G. Moseley, "Laboratory methods for estimating nutritive quality," in *Sward Measurement Handbook*, A. Davies, R. D. Baker, S. A. Grant, and A. S. Laidlaw, Eds., 2nd ed. U.K.: British Grassland Society, 1993, pp. 265–283.

[10] N. Vigneau, M. Ecarnot, G. Rabatel, and P. Roumet, "Potential of field hyperspectral imaging as a non destructive method to assess leaf nitrogen content in wheat," *Field Crops Res.*, vol. 122, no. 1, pp. 25–31, Apr. 2011.

[11] Y. He *et al.*, "Quantitative analysis of nutrient elements in soil using single and double-pulse laser-induced breakdown spectroscopy," *Sensors*, vol. 18, no. 5, May 2018, Art. no. 1526.

[12] D. A. Chang and C.W. Laird, "Near-infrared reflectance spectroscopic analysis of soil C and N," *Soil Sci.*, vol. 167, pp. 110–116, 2002.

[13] P. Zhou, Y. Zhang, W. Yang, M. Li, Z. Liu, and X. Liu, "Development and performance test of an in-situ soil total nitrogen-soil moisture detector based on near-infrared spectroscopy," *Comput. Electron. Agriculture*, vol. 160, pp. 51–58, May 2019.

[14] L. Zhu *et al.*, "A novel method for soil organic matter determination by using an artificial olfactory system," *Sensors*, vol. 19, no. 15, Aug. 2019, Art. no. 3417.

[15] P. Nie, T. Dong, Y. He, and F. Qu, "Detection of soil nitrogen using near infrared sensors based on soil pretreatment and algorithms," *Sensors*, vol. 17, no. 5, May 2017, Art. no. 1102.

[16] L. Liu, M. Ji, and M. Buchroithner, "Transfer learning for soil spectroscopy based on convolutional neural networks and its application in soil clay content mapping using hyperspectral imagery," *Sensors*, vol. 18, no. 9, Sep. 2018, Art. no. 3169.

[17] Y.-Q. Song, X. Zhao, H.-Y. Su, B. Li, Y.-M. Hu, and X.-S. Cui, "Predicting spatial variations in soil nutrients with hyperspectral remote sensing at regional scale," *Sensors*, vol. 18, no. 9, Sep. 2018, Art. no. 3086.

[18] H. Li, S. Jia, and Z. Le, "Quantitative analysis of soil total nitrogen using hyperspectral imaging technology with extreme learning machine," *Sensors*, vol. 19, no. 20, Oct. 2019, Art. no. 4355.

[19] Y. Wang *et al.*, "Qualitative and quantitative diagnosis of nitrogen nutrition of tea plants under field condition using hyperspectral imaging coupled with chemometrics," *J. Sci. Food Agriculture*, vol. 100, no. 1, pp. 161–167, Jan. 2020.

[20] A. Hornero *et al.*, "Monitoring the incidence of Xylella fastidiosa infection in olive orchards using ground-based evaluations, airborne imaging spectroscopy and Sentinel-2 time series through 3-D radiative transfer modelling," *Remote Sens. Environ.*, vol. 236, Jan. 2020, Art. no. 111480.

[21] R. C. Dalal and R. J. Henry, "Simultaneous determination of moisture, organic carbon, and total nitrogen by near infrared reflectance spectrophotometry," *Soil Sci. Soc. Amer. J.*, vol. 50, no. 1, pp. 120–123, Jan. 1986.

[22] M. J. Morra, M. H. Hall, and L. L. Freeborn, "Carbon and nitrogen analysis of soil fractions using near-infrared reflectance spectroscopy," *Soil Sci. Soc. Amer. J.*, vol. 55, no. 1, pp. 288–291, Jan. 1991.

[23] M. Ehsani, M. R. Upadhyaya, S. K. Slaughter, D. Shafii, and S. Pelletier, "A NIR technique for rapid determination of soil mineral nitrogen," *Precis. Agriculture*, vol. 1, pp. 219–236, 1999.

[24] J. G. Scharf *et al.*, "Remote sensing for nitrogen management," *J. Soil Water Conserv.*, vol. 57, pp. 518–524, 2002.

[25] L. Cécillon *et al.*, "Assessment and monitoring of soil quality using near-infrared reflectance spectroscopy (NIRS)," *Eur. J. Soil Sci.*, vol. 60, no. 5, pp. 770–784, Oct. 2009.

[26] P. Chen, D. Haboudane, N. Tremblay, J. Wang, P. Vigneault, and B. Li, "New spectral indicator assessing the efficiency of crop nitrogen treatment in corn and wheat," *Remote Sens. Environ.*, vol. 114, no. 9, pp. 1987–1997, Sep. 2010.

[27] M. Nocita, L. Kooistra, M. Bachmann, A. Müller, M. Powell, and S. Weel, "Predictions of soil surface and topsoil organic carbon content through the use of laboratory and field spectroscopy in the Albany Thicket Biome of Eastern Cape Province of South Africa," *Geoderma*, vol. 167–168, pp. 295–302, Nov. 2011.

[28] M. Vohland, J. Besold, J. Hill, and H.-C. Fründ, "Comparing different multivariate calibration methods for the determination of soil organic carbon pools with visible to near infrared spectroscopy," *Geoderma*, vol. 166, no. 1, pp. 198–205, Oct. 2011.

[29] Z. Sun, Y. Zhang, J. Li, and W. Zhou, "Spectroscopic determination of soil organic carbon and total nitrogen content in pasture soils," *Commun. Soil Sci. Plant Anal.*, vol. 45, no. 8, pp. 1037–1048, Apr. 2014.

[30] X. E. Pantazi, D. Moshou, R. Oberti, J. West, A. M. Mouazen, and D. Bochtis, "Detection of biotic and abiotic stresses in crops by using hierarchical self organizing classifiers," *Precis. Agriculture*, vol. 18, no. 3, pp. 383–393, Jun. 2017.

[31] Y. Peng, L. Zhao, Y. Hu, G. Wang, L. Wang, and Z. Liu, "Prediction of soil nutrient contents using visible and near-infrared reflectance spectroscopy," *ISPRS Int. J. Geo-Inf.*, vol. 8, no. 10, Oct. 2019, Art. no. 437.

[32] Y. Zhou *et al.*, "Fine-resolution mapping of soil total nitrogen across China based on weighted model averaging," *Remote Sens.*, vol. 12, no. 1, Dec. 2019, Art. no. 85.

[33] H. Liu, H. Zhu, Z. Li, and G. Yang, "Quantitative analysis and hyperspectral remote sensing of the nitrogen nutrition index in winter wheat," *Int. J. Remote Sens.*, vol. 41, no. 3, pp. 858–881, Feb. 2020.

[34] A. K. Patel, J. K. Ghosh, and S. U. Sayyad, "Fractional abundances study of macronutrients in soil using hyperspectral remote sensing," *Geocarto Int.*, pp. 1–20, Feb. 2020, doi: 10.1080/10106049.2020.1720315.

[35] B. Stenberg, R. A. Viscarra Rossel, A. M. Mouazen, and J. Wetterlind, "Visible and near infrared spectroscopy in soil science," in *Proc. Adv. Agronomy*, 2010, pp. 163–215.

[36] Y. Ge, J. A. Thomasson, and R. Sui, "Remote sensing of soil properties in precision agriculture: A review," *Front. Earth Sci.*, vol. 5, pp. 229–238, Jun. 2011.

[37] J. M. Soriano-Disla, L. J. Janik, R. A. Viscarra Rossel, L. M. Macdonald, and M. J. McLaughlin, "The performance of visible, near-, and mid-infrared reflectance spectroscopy for prediction of soil physical, chemical, and biological properties," *Appl. Spectroscopy Rev.*, vol. 49, no. 2, pp. 139–186, Feb. 2014.

[38] R. N. Sahoo, S. S. Ray, and K. R. Manjunath, "Hyperspectral remote sensing of agriculture," *Current Sci.*, vol. 108, no. 5, pp. 848–859.

[39] A. Telmo *et al.*, "Hyperspectral imaging: A review on UAV-based sensors, data processing and applications for agriculture and forestry," *Remote Sens.*, vol. 9, no. 11, Oct. 2017, Art. no. 1110.

[40] A. Chlingaryan, S. Sukkarieh, and B. Whelan, "Machine learning approaches for crop yield prediction and nitrogen status estimation in precision agriculture: A review," *Comput. Electron. Agriculture*, vol. 151, pp. 61–69, Aug. 2018.

[41] L. Sun, F. Wu, T. Zhan, W. Liu, J. Wang, and B. Jeon, "Weighted nonlocal low-rank tensor decomposition method for sparse unmixing of hyperspectral images," *IEEE J. Sel. Topics Appl. Earth Observ. Remote Sens.*, vol. 13, no. 1, pp. 1174–1188, Mar. 2020, doi: 10.1109/JSTARS.2020.2980576.

[42] Y. Yuan, Z. Zhang, and Q. Wang, "Improved collaborative non-negative matrix factorization and total variation for hyperspectral unmixing," *IEEE J. Sel. Topics Appl. Earth Observ. Remote Sens.*, vol. 13, pp. 998–1010, Mar. 2020, doi: 10.1109/JSTARS.2020.2977399.

[43] N. Keshava and J. F. Mustard, "Spectral unmixing," *IEEE Signal Process. Mag.*, vol. 19, no. 1, pp. 44–57, Jan. 2002.

[44] R. N. Clark *et al.*, "USGS digital spectral library splib06a," US Geol. Surv. Digit. data Ser. 231, 2007. [Online]. Available: http://speclab.cr.usgs.gov/spectral.lib06

[45] B. Somers, G. P. Asner, L. Tits, and P. Coppin, "Endmember variability in spectral mixture analysis: A review," *Remote Sens. Environ.*, vol. 115, no. 7, pp. 1603–1616.

[46] J. M. Bioucas-Dias *et al.*, "Hyperspectral unmixing overview: Geometrical, statistical, and sparse regression-based approaches," *IEEE J. Sel. Topics Appl. Earth Observ. Remote Sens.*, vol. 5, no. 2, pp. 354–379, Apr. 2012.

[47] R. Heylen, M. Parente, and P. Gader, "A review of nonlinear hyperspectral unmixing methods," *IEEE J. Sel. Topics Appl. Earth Observ. Remote Sens.*, vol. 7, no. 6, pp. 1844–1868, Jun. 2014.

[48] A. Zare and K. C. Ho, "Endmember variability in hyperspectral analysis: Addressing spectral variability during spectral unmixing," *IEEE Signal Process. Mag.*, vol. 31, no. 1, pp. 95–104, Jan. 2014.

[49] N. Gillis and R. Luce, "A fast gradient method for nonnegative sparse regression with self-dictionary," *IEEE Trans. Image Process.*, vol. 27, no. 1, pp. 24–37, Jan. 2018.

[50] S. Khoshsokhan, R. Rajabi, and H. Zayyani, "Sparsity-constrained distributed unmixing of hyperspectral data," *IEEE J. Sel. Topics Appl. Earth Observ. Remote Sens.*, vol. 12, no. 4, pp. 1279–1288, Apr. 2019.

[51] C. Li *et al.*, "Sparse unmixing of hyperspectral data with bandwise model," *Inf. Sci.*, vol. 512, pp. 1424–1441, Feb. 2020.

[52] U. B. Gewali, S. T. Monteiro, and E. Saber, "Machine learning based hyperspectral image analysis: A survey," 2018, *arXiv1802.08701*.

[53] C. C. Borel and S. A. Gerstl, "Nonlinear spectral mixing models for vegetative and soil surfaces," *Remote Sens. Environ.*, vol. 47, no. 3, pp. 403–416, Mar. 1994.

[54] W. Fan, B. Hu, J. Miller, and M. Li, "Comparative study between a new nonlinear model and common linear model for analysing laboratory simulated-forest hyperspectral data," *Int. J. Remote Sens.*, vol. 30, no. 11, pp. 2951–2962, Jun. 2009.

[55] A. Halimi, Y. Altmann, N. Dobigeon, and J.-Y. Tourneret, "Nonlinear unmixing of hyperspectral images using a generalized bilinear model," *IEEE Trans. Geosci. Remote Sens.*, vol. 49, no. 11, pp. 4153–4162, Nov. 2011.

[56] N. Dobigeon, J.-Y. Tourneret, C. Richard, J. C. M. Bermudez, S. McLaughlin, and A. O. Hero, "Nonlinear unmixing of hyperspectral images: Models and algorithms," *IEEE Signal Process. Mag.*, vol. 31, no. 1, pp. 82–94, Jan. 2014.

[57] B. Yang, B. Wang, and Z. Wu, "Nonlinear hyperspectral unmixing based on geometric characteristics of bilinear mixture models," *IEEE Trans. Geosci. Remote Sens.*, vol. 56, no. 2, pp. 694–714, Feb. 2018.

[58] X. Xu, Z. Shi, and B. Pan, "$\ell 0$-based sparse hyperspectral unmixing using spectral information and a multi-objectives formulation," *ISPRS J. Photogramm. Remote Sens.*, vol. 141, pp. 46–58, Jul. 2018.

[59] J. Nascimento and G. Martín, "Nonlinear spectral unmixing," in *Proc. Data Handling Sci. Technol.*, 2020, pp. 151–166.

[60] P. L. Antonio, A. V. R. Raphael, A. Pietro, and B. Andrea, "Prediction of soil properties with PLSR and vis-NIR spectroscopy: Application to mediterranean soils from Southern Italy," *Current Anal. Chem.*, vol. 8, no. 2, pp. 283–299, Apr. 2012.

[61] R. Casa, F. Castaldi, S. Pascucci, B. Basso, and S. Pignatti, "Geophysical and hyperspectral data fusion techniques for in-field estimation of soil properties," *Vadose Zone J.*, vol. 12, no. 4, Nov. 2013, Art. no. vzj2012.0201.

[62] F. Cao, Z. Yang, J. Ren, M. Jiang, and W.-K. Ling, "Linear vs. nonlinear extreme learning machine for spectral-spatial classification of hyperspectral images," *Sensors*, vol. 17, no. 11, Nov. 2017, Art. no. 2603.

[63] X. Shen, W. Bao, and K. Qu, "Spatial-spectral hyperspectral endmember extraction using a spatial energy prior constrained maximum simplex volume approach," *IEEE J. Sel. Topics Appl. Earth Observ. Remote Sens.*, vol. 13, pp. 1347–1361, Apr. 2020, doi: 10.1109/JSTARS.2020.2981402.

[64] K. J. Guilfoyle, M. L. Althouse, and C.-I. Chang, "A quantitative and comparative analysis of linear and nonlinear spectral mixture models using radial basis function neural networks," *IEEE Trans. Geosci. Remote Sens.*, vol. 39, no. 10, pp. 2314–2318, Oct. 2001.

[65] J. Chen, C. Richard, and P. Honeine, "Nonlinear unmixing of hyperspectral data based on a linear-mixture/nonlinear-fluctuation model," *IEEE Trans. Signal Process.*, vol. 61, no. 2, pp. 480–492, Jan. 2013.

[66] C. Fevotte and N. Dobigeon, "Nonlinear hyperspectral unmixing with robust nonnegative matrix factorization," *IEEE Trans. Image Process.*, vol. 24, no. 12, pp. 4810–4819, Dec. 2015.

[67] N. Dobigeon, Y. Altmann, N. Brun, and S. Moussaoui, "Linear and nonlinear unmixing in hyperspectral imaging," in *Proc. Data Handling Sci. Technol.*, 2016, pp. 185–224.

[68] B. Ayerdi and M. Graña, "Hyperspectral image nonlinear unmixing and reconstruction by ELM regression ensemble," *Neurocomputing*, vol. 174, pp. 299–309, Jan. 2016.

[69] A. Halimi, J. M. Bioucas-Dias, N. Dobigeon, G. S. Buller, and S. McLaughlin, "Fast hyperspectral unmixing in presence of nonlinearity or mismodeling effects," *IEEE Trans. Comput. Imag.*, vol. 3, no. 2, pp. 146–159, Jun. 2017.

[70] M. Wang, M. Zhao, J. Chen, and S. Rahardja, "Nonlinear unmixing of hyperspectral data via deep autoencoder networks," *IEEE Geosci. Remote Sens. Lett.*, vol. 16, no. 9, pp. 1467–1471, Sep. 2019.

[71] R. A. V. Rossel and T. Behrens, "Using data mining to model and interpret soil diffuse reflectance spectra," *Geoderma*, vol. 158, no. 1–2, pp. 46–54, Aug. 2010.

[72] A. Stevens, M. Nocita, G. Tóth, L. Montanarella, and B. van Wesemael, "Prediction of soil organic carbon at the European scale by visible and near infrared reflectance spectroscopy," *PLoS One*, vol. 8, no. 6, Jun. 2013, Art. no. e66409.

[73] A. Morellos *et al.*, "Machine learning based prediction of soil total nitrogen, organic carbon and moisture content by using VIS-NIR spectroscopy," *Biosyst. Eng.*, vol. 152, pp. 104–116, 2016.

[74] J. Padarian, B. Minasny, and A. B. McBratney, "Using deep learning to predict soil properties from regional spectral data," *Geoderma Regional*, vol. 16, Mar. 2019, Art. no. e00198.

[75] T. Chen, Q. Chang, J. Liu, J. G. P. W. Clevers, and L. Kooistra, "Identification of soil heavy metal sources and improvement in spatial mapping based on soil spectral information: A case study in northwest China," *Sci. Total Environ.*, vol. 565, pp. 155–164, Sep. 2016.

[76] H. Liu, T. Shi, Y. Chen, J. Wang, T. Fei, and G. Wu, "Improving spectral estimation of soil organic carbon content through semi-supervised regression," *Remote Sens.*, vol. 9, no. 1, Jan. 2017, Art. no. 29.

[77] B. Minasny and A. B. McBratney, "Regression rules as a tool for predicting soil properties from infrared reflectance spectroscopy," *Chemometrics Intell. Lab. Syst.*, vol. 94, no. 1, pp. 72–79, Nov. 2008.

[78] M. C. Sarathjith, B. S. Das, S. P. Wani, and K. L. Sahrawat, "Variable indicators for optimum wavelength selection in diffuse reflectance spectroscopy of soils," *Geoderma*, vol. 267, pp. 1–9, Apr. 2016.

[79] R. Duca and F. Del Frate, "Hyperspectral and multiangle CHRIS–PROBA images for the generation of land cover maps," *IEEE Trans. Geosci. Remote Sens.*, vol. 46, no. 10, pp. 2857–2866, Oct. 2008.

[80] J. Plaza, A. Plaza, R. Perez, and P. Martinez, "On the use of small training sets for neural network-based characterization of mixed pixels in remotely sensed hyperspectral images," *Pattern Recognit.*, vol. 42, no. 11, pp. 3032–3045, Nov. 2009.

[81] G. A. Licciardi and F. F. Del, "Pixel unmixing in hyperspectral data by means of neural networks," *IEEE Trans. Geosci. Remote Sens.*, vol. 49, no. 11, pp. 4163–4172, Nov. 2011.

[82] R. A. Borsoi, T. Imbiriba, and J. C. M. Bermudez, "Deep generative endmember modeling: An application to unsupervised spectral unmixing," *IEEE Trans. Comput. Imag.*, vol. 6, pp. 374–384, Oct. 2020, doi: 10.1109/TCI.2019.2948726.

[83] A. Elshamli, G. W. Taylor, A. Berg, and S. Areibi, "Domain adaptation using representation learning for the classification of remote sensing images," *IEEE J. Sel. Topics Appl. Earth Observ. Remote Sens.*, vol. 10, no. 9, pp. 4198–4209, Sep. 2017.

[84] A. Ben Hamida, A. Benoit, P. Lambert, and C. Ben Amar, "3-D deep learning approach for remote sensing image classification," *IEEE Trans. Geosci. Remote Sens.*, vol. 56, no. 8, pp. 4420–4434, Aug. 2018.

[85] M. E. Paoletti, J. M. Haut, J. Plaza, and A. Plaza, "Deep learning classifiers for hyperspectral imaging: A review," *ISPRS J. Photogramm. Remote Sens.*, vol. 158, pp. 279–317, Dec. 2019.

[86] Y. Su, J. Li, A. Plaza, A. Marinoni, P. Gamba, and S. Chakravortty, "DAEN: Deep autoencoder networks for hyperspectral unmixing," *IEEE Trans. Geosci. Remote Sens.*, vol. 57, no. 7, pp. 4309–4321, Jul. 2019.

[87] S. Bera and V. K. Shrivastava, "Analysis of various optimizers on deep convolutional neural network model in the application of hyperspectral remote sensing image classification," *Int. J. Remote Sens.*, vol. 41, no. 7, pp. 2664–2683, Apr. 2020.

[88] X. Zhou, J. Sun, Y. Tian, B. Lu, Y. Hang, and Q. Chen, "Development of deep learning method for lead content prediction of lettuce leaf using hyperspectral images," *Int. J. Remote Sens.*, vol. 41, no. 6, pp. 2263–2276, Mar. 2020.

[89] N. C. Wollenhaupt, D. J. Mulla, and C. A. Gotway, "Soil sampling and interpolation techniques for mapping spatial variability of soil properties," in *Proc. State Site Specific Manage. Agriculture*, 1997, pp. 19–53.

[90] B. C. O'Kelly, "Accurate determination of moisture content of organic soils using the oven drying method," *Drying Technol.*, vol. 22, no. 7, pp. 1767–1776.

[91] T. H. Roy RN, A. Finck, and G. J. Blair, Plant nutrition for food security. A guide for integrated nutrient management. FAO Fertilizer and Plant Nutrition Bulletin, 2006.

[92] L. Taiz and E. Zeiger, "Plant physiology," *Ann. Botany*, vol. 91, 3rd ed., no. 6, pp. 750–751, May 2003.

[93] L. Weidong, F. Baret, G. Xingfa, T. Qingxi, Z. Lanfen, and Z. Bing, "Relating soil surface moisture to reflectance," *Remote Sens. Environ.*, vol. 81, no. 2/3, pp. 238–246, Aug. 2002.

[94] J. Bao, M. Chi, and J. A. Benediktsson, "Spectral derivative features for classification of hyperspectral remote sensing images: Experimental evaluation," *IEEE J. Sel. Topics Appl. Earth Observ. Remote Sens.*, vol. 6, no. 2, pp. 594–601, Apr. 2013.

[95] F. Tsai and W. Philpot, "Derivative analysis of hyperspectral data," *Remote Sens. Environ.*, vol. 66, no. 1, pp. 41–51, 1998.

[96] J. Zhang, B. Rivard, and A. Sanchez-Azofeifa, "Derivative spectral unmixing of hyperspectral data applied to mixtures of lichen and rock," *IEEE Trans. Geosci. Remote Sens.*, vol. 42, no. 9, pp. 1934–1940, Sep. 2004.

[97] R. N. Clark and T. L. Roush, "Reflectance spectroscopy: Quantitative analysis techniques for remote sensing applications," *J. Geophys. Res. Solid Earth*, vol. 89, no. B7, pp. 6329–6340, Jul. 1984.

[98] C. Hecker, F. J. A. van Ruitenbeek, H. M. A. van der Werff, W. H. Bakker, R. D. Hewson, and F. D. van der Meer, "Spectral absorption feature analysis for finding ore: A tutorial on using the method in geological remote sensing," *IEEE Geosci. Remote Sens. Mag.*, vol. 7, no. 2, pp. 51–71, Jun. 2019.

[99] N. Keshava, "A survey of spectral unmixing algorithms," *Lincoln Lab. J.*, vol. 14, no. 1, pp. 55–78, 2003, [Online]. Available: http://citeseerx.ist.psu.edu/viewdoc/download?doi=10.1.1.69.7411&rep=rep1&type=pdf

[100] J. B. Adams, M. O. Smith, and P. E. Johnson, "Spectral mixture modeling: A new analysis of rock and soil types at the Viking Lander 1 Site," *J. Geophys. Res.*, vol. 91, no. B8, 1986, Art. no. 8098.

[101] G. D. Robinson, H. N. Gross, and J. R. Schott, "Evaluation of two applications of spectral mixing models to image fusion," *Remote Sens. Environ.*, vol. 71, no. 3, pp. 272–281, Mar. 2000.

[102] B. D. Ripley, *Pattern Recognition and Neural Networks*. Cambridge, U.K.: Cambridge Univ. Press, 2007.

[103] A. Clesceri, L. Greenberg, and A. Eaton, *Standard Methods for the Examination of Water and Wastewater*. Washington, DC, USA: Amer. Public Health Assoc., 1999, p. 733.

[104] "D8001-16e1 standard test method for determination of total nitrogen, total Kjeldahl nitrogen by calculation, and total phosphorus in water, wastewater by ion chromatography," ASTM Int., West Conshohocken, PA, USA, 2016, p. 11. [Online]. Available: https://doi.org/10.1520/D8001-16E01

[105] J. Weiss and T. Weiss, *Handbook of Ion Chromatography*. New York, NY, USA: Wiley, 2005.

[106] K. Ito, Y. Takayama, N. Makabe, R. Mitsui, and T. Hirokawa, "Ion chromatography for determination of nitrite and nitrate in seawater using monolithic ODS columns," *J. Chromatogr. A*, vol. 1083, no. 1/2, pp. 63–67, Aug. 2005.

[107] P. R. Haddad, P. N. Nesterenko, and W. Buchberger, "Recent developments and emerging directions in ion chromatography," *J. Chromatogr. A*, vol. 1184, no. 1–2, pp. 456–473, Mar. 2008.

[108] E. Ben-Dor and A. Banin, "Near-infrared analysis as a rapid method to simultaneously evaluate several soil properties," *Soil Sci. Soc. Amer. J.*, vol. 59, no. 2, 1995, Art. no. 364.

[109] K. D. Shepherd and M. G. Walsh, "Development of reflectance spectral libraries for characterization of soil properties," *Soil Sci. Soc. Amer. J.*, vol. 66, no. 3, 2002, Art. no. 988.

[110] E. Ben-Dor, N. Goldlshleger, Y. Benyamini, M. Agassi, and D. G. Blumberg, "The spectral reflectance properties of soil structural crusts in the 1.2- to 2.5-μm spectral region," *Soil Sci. Soc. Amer. J.*, vol. 67, no. 1, pp. 289–299, Jan. 2003.

[111] F. Castaldi, A. Palombo, F. Santini, S. Pascucci, S. Pignatti, and R. Casa, "Evaluation of the potential of the current and forthcoming multispectral and hyperspectral imagers to estimate soil texture and organic carbon," *Remote Sens. Environ.*, vol. 179, pp. 54–65, Jun. 2016.

[112] R. J. Murphy and S. T. Monteiro, "Mapping the distribution of ferric iron minerals on a vertical mine face using derivative analysis of hyperspectral imagery (430–970 nm)," *ISPRS J. Photogramm. Remote Sens.*, vol. 75, pp. 29–39, Jan. 2013.

[113] J. Tian and W. D. Philpot, "Relationship between surface soil water content, evaporation rate, and water absorption band depths in SWIR reflectance spectra," *Remote Sens. Environ.*, vol. 169, pp. 280–289, 2015.

[114] P. H. Fidêncio, R. J. Poppi, J. C. de Andrade, and H. Cantarella, "Determination of organic matter in soil using near-infrared spectroscopy and partial least squares regression," *Commun. Soil Sci. Plant Anal.*, vol. 33, no. 9–10, pp. 1607–1615, May 2002.

[115] S. J. Gaffey, "Spectral reflectance of carbonate minerals in the visible and near infrared (0.35–2.55 microns); calcite, aragonite, and dolomite," *Amer. Mineral.*, vol. 71, no. 1–2, pp. 151–162, 1986.

[116] G. R. Hunt, "Visible and near-infrared spectra of minerals and rocks: III. Oxides and hydro-oxides," *Modern Geol.*, vol. 2, pp. 195–205, 1971.

[117] E. Ben-Dor, Y. Inbar, and Y. Chen, "The reflectance spectra of organic matter in the visible near-infrared and short wave infrared region (400–2500 nm) during a controlled decomposition process," *Remote Sens. Environ.*, vol. 61, no. 1, pp. 1–15, Jul. 1997.

[118] G. R. Hunt, "Visible and near-infrared spectra of minerals and rocks: VI. Additional silicates," *Modern Geol.*, vol. 4, pp. 85–106, 1973.

[119] G. R. Hunt, "Spectroscopic properties of rocks and minerals," in *Handbook of Physical Properties of Rocks*, Robert S. Carmichael, Ed. Boca Raton, FL, USA: CRC Press, 1982, pp. 295–386.

[120] S. J. Gaffey, "Spectral reflectance of carbonate minerals in the visible and near infrared (0.35–2.55 μm): Anhydrous carbonate minerals," *J. Geophys. Res.*, vol. 92, no. B2, 1987, Art. no. 1429.

[121] G. Zheng, C. Jiao, S. Zhou, and G. Shang, "Analysis of soil chronosequence studies using reflectance spectroscopy," *Int. J. Remote Sens.*, vol. 37, no. 8, pp. 1881–1901, Apr. 2016.

[122] L. Zhao *et al.*, "Assessing the utility of visible-to-shortwave infrared reflectance spectroscopy for analysis of soil weathering intensity and paleoclimate reconstruction," *Palaeogeogr. Palaeoclimatol. Palaeoecol.*, vol. 512, pp. 80–94, Dec. 2018.

[123] C. Wang *et al.*, "Rapid and accurate evaluation of the quality of commercial organic fertilizers using near infrared spectroscopy," *PLoS One*, vol. 9, no. 2, Feb. 2014, Art. no. e88279.

[124] S. Chabrillat, A. F. Goetz, L. Krosley, and H. W. Olsen, "Use of hyperspectral images in the identification and mapping of expansive clay soils and the role of spatial resolution," *Remote Sens. Environ.*, vol. 82, no. 2–3, pp. 431–445, Oct. 2002.

[125] R. A. Viscarra Rossel *et al.*, "A global spectral library to characterize the world's soil," *Earth-Sci. Rev.*, vol. 155, pp. 198–230, Apr. 2016.

[126] Y. Glorot, X. Bordes, and A. Bengio, "Deep sparse rectifier neural networks," in *Proc. 14th Int. Conf. Artif. Intell. Statist.*, 2011, pp. 315–323.

Ajay Kumar Patel (Student Member, IEEE) received the bachelor's degree in electronics and communication engineering from Rajiv Gandhi Technical University, Bhopal, India, in 2009 and the M.Tech. degree in geoinformatics and natural resources engineering from the Indian Institute of Technology, Bombay, Mumbai, India, in 2013. He is currently working toward the Ph.D. degree with the Geomatics Engineering Group, Indian Institute of Technology Roorkee, Roorkee, India.

His research interests include satellite image processing and hyperspectral remote sensing using deep learning techniques.

Jayanta Kumar Ghosh received the bachelor's degree from the Indian Institute of Engineering Science and Technology, Howrah, India, in 1984, the master's degree from the Indian Institute of Technology Kanpur, Kanpur, India, in 1990, and the doctoral degree from the Indian Institute of Technology Roorkee, Roorkee, India, in 1997, all in civil engineering.

He is currently a Professor with the Civil Engineering Department (Geomatics Engineering Group), Indian Institute of Technology Roorkee. He is engaged in teaching, research, and consultancy works in geomatics engineering for more than 35 years. He has authored or coauthored more than 110 publications in international and national journals of repute and conferences. He is an author of two books titled *Elementary Engineering Surveying* (Studium Press, 2006) and A Text Book on GPS Surveying (CRC Press, 2016).

Dr. Ghosh is a member of different national and international technical societies. He has bagged many national and international laurels in his academic career.

Shivam Pande (Student Member, IEEE) received the B.Tech. degree in civil engineering from the Maulana National Institute of Technology, Bhopal, India, in 2015 and the M.Tech. degree in geoinformatics and civil engineering from the Indian Institute of Technology Kanpur, Kanpur, India, in 2018. He is currently working toward the Ph.D. degree with the Centre of Studies in Resources Engineering, Indian Institute of Technology Bombay, Mumbai, India under Prime Minister Research Fellowship (PMRF – 2018).

His research focuses on processing on remote sensing imageries using deep learning techniques.

Sameer Usmangani Sayyad received the bachelor's degree in civil engineering from the Dr J J Magdum College of Engineering, Jaisingpur, India, in 2003 and the M.E. degree in environmental engineering from the Walchand College of Engineering, Sangli, India, in 2009.

He is currently an Assistant Professor with the Civil and Environmental Engineering Department, Veermata Jijabai Technological Institute, Mumbai, India. He is a part-time Research Scholar with the Civil Engineering Department, Environmental Engineering Group, Indian Institute of Technology Roorkee, Roorkee, India. His research interests include membrane separation processes for industrial wastewater treatment and reuse with special emphasis on forward osmosis and reverse osmosis processes.